

ASSOCIATION EURATOM - UNIVERSITY OF LATVIA
AEUL



ANNUAL REPORT 2009

Riga 2010

TABLE OF CONTENT

FOREWORD

1. INTRODUCTION	4
2. FUSION PROGRAMME ORGANISATION.....	5
2.1. Programme Objectives	5
2.2. Association EURATOM-University of Latvia	5
2.3. Fusion Research Units	5
2.4. Association Steering Committee	6
2.5. The Latvian Members in the EU Fusion Committees.....	6
2.6. Funding and Research Volume 2009	
3. PHYSICS PROGRAMME – FUSION PHYSICS	7
3.1. Development of a gallium jet limiter (GJL) as a system for protection of plasma facing components ensuring the removal of the deposited heat and impurities.....	7
3.2. Characterization of the impurity concentration, profiling and erosion in ITER relevant materials	13
3.3. Theory and Code Development	
3.3.1. Stochastization of magnetic fields and magnetic reconnection.....	45
3.3.2. Radiation stability of reactor materials	47
4. EFDA FUSION TECHNOLOGY PROGRAMME	52
4.1. Analysis of tritium distribution in carbon-based plasma-facing components	52
5. STAFF MOBILITY ACTIONS	60
5.1. Staff Mobility Visits	60
6. OTHER ACTIVITIES	60
6.1. Conferences, Workshops and Meetings	60
6.2. Telephone conferences	61
7. PUBLICATIONS 2009	61

7.1. Fusion Physics and Plasma Engineering	61
7.1.1. Publications in scientific journals	61
7.1.2. Conference articles	62
7.2. Fusion Technology	62
7.2.1. Publications in scientific journals	62

1. INTRODUCTION

This Annual Report summarizes the fusion research activities of the Latvian Research Unit of the Association EURATOM-University of Latvia in 2009.

The activities of the Research Unit are divided in the Fusion Physics Programme and Technology under the Contract of Association and Technology Programme under EFDA. In the frame of the EFDA Workprogramme 2008 the AEUL was included in the Goal Oriented Training Programme EUROBREED, and on the 1st September 2009 the trainee started to take part in the programme.

The Physics Programme is carried out at IP UL – Institute of Physics, University of Latvia, and at ISSP UL – Institute of Solid State Physics, University of Latvia. The research areas of the Physics Programme are:

- Preparation of a gallium jet limiter for testing under reactor relevant conditions
- Characterization of the impurity concentration, profiling and erosion in ITER relevant materials using laser ablation spectroscopy
- LIBS spectroscopy of the impurity concentration depth profile in wall tiles
- Theory and Code Development.

The Technology Programme is carried out at ICP UL - Institute of Chemical Physics, University of Latvia. The technology research and development under EFDA JET is focused on the analysis of tritium distribution in plasma facing components.

Several Staff Mobility actions took place in 2009: to IPP Garching, FZK Karlsruhe, UKAEA Culham, and ISTOK Lisbon.

The 13th European Fusion Theory Conference was held in Riga, Latvia, 12-15 October. The conference was organized by the Association "EURATOM - University of Latvia".

2. FUSION PROGRAMME ORGANISATION

2.1 Programme Objectives

The Latvian Fusion Programme, under the Association EURATOM-University of Latvia, is fully integrated into the European Programme, which has set the long-term aim of the joint creation of prototype reactors for power stations to meet the needs of society: operational safety, environmental compatibility and economic viability. The objectives of the Latvian programme are: (i) to carry out high-level scientific and technological research in the field of nuclear fusion, (ii) to make a valuable and visible contribution to the European Fusion Programme and to the international ITER Project in our focus areas. This can be achieved by close collaboration with other Associations.

2.2 Association EURATOM-University of Latvia

The Latvian contribution to the European fusion programme began in 2000 in the form of cost-sharing actions (fixed contribution contracts with EURATOM). The Association was established on 19 December 2001 incorporating the existing cost-sharing actions into its work plan.

2.3 Fusion Research Units

The Latvian Research Unit of the Association EURATOM-University of Latvia consists of three Institutes of University of Latvia.

1. IP UL – Institute of Physics, University of Latvia
32 Miera St., Salaspils LV-2169, Latvia.
Phone +371 6 7944700, Fax. +371 6 7901214
2. ISSP UL – Institute of Solid State Physics, University of Latvia
8 Kengaraga St., Riga LV-1063, Latvia.
Phone +371 6 7187810, Fax. +371 6 7132778
3. ICP UL - Institute of Chemical Physics, University of Latvia

4 Kronvalda Blvd., Riga LV-1010, Latvia.
Phone +371 6 7033884, Fax. +371 6 7033884

2.4 Association Steering Committee

The research activities of the Latvian Association EURATOM-University of Latvia are directed by the Steering Committee, which comprises the following members in 2008:

Mr. Douglas Bartlett, EU Commission, Fusion association agreements, Unit J4, DG Research.

Mr. Steven Booth, Fusion association agreements, Unit J4, DG Research

Mr. Marc Pipeleers, Administration and finance, Unit J5, DG Research

Mrs. Maija Bundule, Ministry of Education and Science

Mr. Ivars Lacis, University of Latvia

Mr. Andrejs Silins, Latvian Academy of Sciences

The Steering Committee had one meeting in 2009, at ISSP UL with remote participation of EU Commission representatives, on July 2, 2009.

2.5 The Latvian Members in the EU Fusion Committees

Consultative Committee for the EURATOM Specific Research and Training Programme in the Field of Nuclear Energy-Fusion (CCE-FU)

Mr. Andris Sternberg, ISSP UL

EFDA Steering Committee

Mr. Andris Sternberg, ISSP UL

Governing Board for the Joint European Undertaking for ITER and the Development of Fusion Energy, "Fusion for Energy" (F4E GB)

Mrs. Maija Bundule, Latvian Academy of Sciences

Mr. Andris Sternberg, ISSP UL

EFDA Public Information Group

Mr. Maris Kundzins, ISSP UL

2.6 Public Information

Conferences

Results of fusion research were presented at:

- the annual scientific conference of University of Latvia,
- International Conference “Functional materials and nanotechnologies” (FM&NT- 2009), Riga, 31st March – 3rd April 2009.
- 13th European fusion theory conference in Riga, 12-15 October, 2009.

Educational activities

Excursions at ISSP UL from schools two to three times a month, PhD students from Latvian universities. Booklets about ISSP UL and EFDA were distributed.

Television, press

Presentations in TV – in popular science telecast..

Presentations in Radio – popular science broadcast..

Popularization of science

Presentation in the TV programme “Science in Latvia”,

Presentation in the programme “Researchers’ Night in Latvia” on 26th of September, 2009.

2.7 Funding and Research Volume 2008

In 2009, the expenditure of the Association EURATOM-University of Latvia was about

481 360 EUR, including Staff Mobility actions

Item	Expenditure (EUR)
General Support (20% EU contribution)	460 301.00
Physics	320 892.00
Technology Tasks EFDA Art. 5.1.a (20% EU contribution)	139 409.00
Missions and Secondments under the Agreement on Staff Mobility (100% EU contribution)	15 059.00
TOTAL	460 301.00
Priority Actions (Additional 20% EU contribution)	6000.00

3. PHYSICS PROGRAMME – FUSION PHYSICS

3.1. Development of a gallium jet limiter (GJL) as a system for protection of plasma facing components ensuring the removal of the deposited heat and impurities.

Principal investigator: E.Platacis

Protection of solid surfaces by liquid metals has been considered as a suitable potential solution of problems associated with the application of solid walls exposed to high power loads. Simultaneously with this an efficient heat transfer and removal can be ensured. In large-scale fusion devices during emergency regimes the thermal loads can reach up to some GW/m^2 . However, as a reference value the load on a full-scale divertor can be estimated at the level of $20\text{-}50 \text{ MW/m}^2$. Protection of the divertor plates by liquid lithium has already been proven as a promising solution mainly because of the high retention rate of H in Li. For comparison: the high-z metals (like Ga) have an advantage mainly due to their low electric conductivity and low evaporation rate. With this the intensity of MHD interaction is reduced and rather fast motion of the liquid metal is feasible under conditions when high intensity heat energy is absorbed. It means that the system can be proposed for large scale devices ensuring heat removal and corresponding evacuating capacity.

In previous years liquid gallium jets were investigated on the tokamak ISTTOK. In 2009, a collaborative paper was published in the *Journal of Nuclear Materials* [1] describing the interaction of a free falling liquid gallium jet with the ISTTOK plasma. The following citations from the abstract are summarizing the achieved results: “ISTTOK has been successfully operated with this jet with no noticeable discharge degradation and no severe effect on the main plasma parameters or a significant plasma contamination by liquid metal. Power extraction capability of the jet is extrapolated from the heat flux profiles measured in the ISTTOK plasmas.” The first estimates show that the corresponding heat loads on the jet are really high and can already be considered as relevant to divertor real situation.

Outcome of the year 2009 directly related to the FTU was finalized during the meeting on December 07-21, 2009 in Frascati. Teams from FTU (Italy) and ISTTOK (Portugal), as well as from IPUL (Latvia), were participating in this meeting. Parties have agreed that a distinct correlation with the conditions in a full-scale divertor should be considered as the basis or *motivation* for the further work on FTU. A fully acceptable correlation was stated:

<u>Jet in a divertor protecting system</u>	<u>Jet in the SOL of FTU.</u>
Liquid metal: Ga, Li	Liquid metal: Ga
Magnetic field: 5-10 T	Magnetic field: 6-8 T
Jet velocity: 5-10 m/s	Jet velocity: 4-6 m/s
Jet diameter: 5-8 mm	Jet diameter: 3-5 mm
Jet length: 0.3-0.4 m	Jet length: 0.3-0.4 m
Power load: $10\text{-}50 \text{ MW/m}^2$	Power load: ??

The question concerning the expected power load in the SOL of FTU formally remains open. As it was mentioned above, the power extraction capability of a jet under the conditions of the ISTTOK plasma has already been evaluated and probably can be chosen as a basis for extrapolation to higher values of the thermal loads.

As an *experimental background* for this the following two achieved results were selected: first, the result that a strong orthogonal magnetic field stabilizes the free falling liquid metal jet; and second, the observations demonstrated that in spite of the intensive action of electromagnetic forces and at high power loads the Ga-jet inside the ISTTOK plasma remains continuous. The most important *question to be clarified* is the deflection of the jet by plasma.

Design proposal presented by IPUL (Fig. 3.1.1) has been accepted as to be feasible. The general scheme remains unchanged, the liquid metal will be introduced through the horizontal side gate and evacuated through the vertical downward directed gate. For the installation the port number 3 was chosen. The feeding system in principle will be equal to its forerunner in ISTTOK and most of the tested and well-proved components will be kept unchanged. Of course, some specific new elements will be needed. For example, an additional upper electromagnetic pump. The jet will be directed into the SOL downwards under 23° angle. Longitudinal displacement of the jet is also foreseen to cover the full thickness of the layer. It is proposed to arrange/dispose the jet introduction assembly in a vacuum tight “pocket” fastened to the outer vacuum flange of the port. In such a way the opportunity arises for the layout of all the components, first of all the “open/shut” valve, as close as possible to the jet-generating nozzle. The passive amount of liquid metal between the valve and the nozzle will be minimized. This amount must be accelerated at each pulse. After passing the SOL the liquid metal will be directed towards a non-conducting reflector, then to the receiver and at the end into the Ga collector. The assembly for linear displacement of the nozzle turns out to be rather complicated. The motion is “introduced” into the vacuum space through bellows and vacuum break. The linear displacement is ensured by a gear screw. The assembly is fastened to the flange of the mentioned “pocket”.

Mock-up of the liquid metal installation for FTU

In comparison with ISTTOK the operation conditions on FTU are significantly more complex. Instead of the length of the jet 10-13 cm its length must be increased up to 30-40 cm, instead of the velocity of the liquid metal jet 2-3 m/s the velocity should be increase up to 4-6 m/s, diameter of the jet $d = 2-3$ mm should be increase up to 3-5 mm. Additionally, the jet must be directed not directly downward but under 23° angle. The setup used for ISTTOK related investigations was essentially modified and partly new-built (Fig.3.1.2). On the left of the scheme (Fig. 3.1.2a) the 1:1 scaled replica of the FTU cross-section is shown. The mock-up itself repeats the part of the cross-section which is marked by the rectangular insert. The new components such as an additional EM pump and a valve with a higher flow coefficient are shown in the middle of the scheme. Fig. 3.1.2b presents a photo of the fully assembled installation.

Fig. 3.1.3 shows all essential units for the jet injection. The walls are made of SS, the front cover is made of transparent Plexiglas (for ensuring visual observations). The configuration of the corner between the horizontal and vertical gates is exactly reproduced since it is considered as the most risky point for an undisturbed injection of the jet. The protective tray is made exchangeable; optimization of this unit belongs to the tasks of this study. The injector is designed for the generation of a single jet as well as for two or three parallel jets. A possibility to change the direction of the jet (the angle of injection) is foreseen.

Finally, Fig. 3.1.4 presents a photo of three jets injected in accordance with the initial boundary conditions, namely, the length, velocity and the inclination of the jet correspond to the requirements. Details of the design, for example, the feeding unit, the honeycomb and the unit for installation of the angle also are shown.

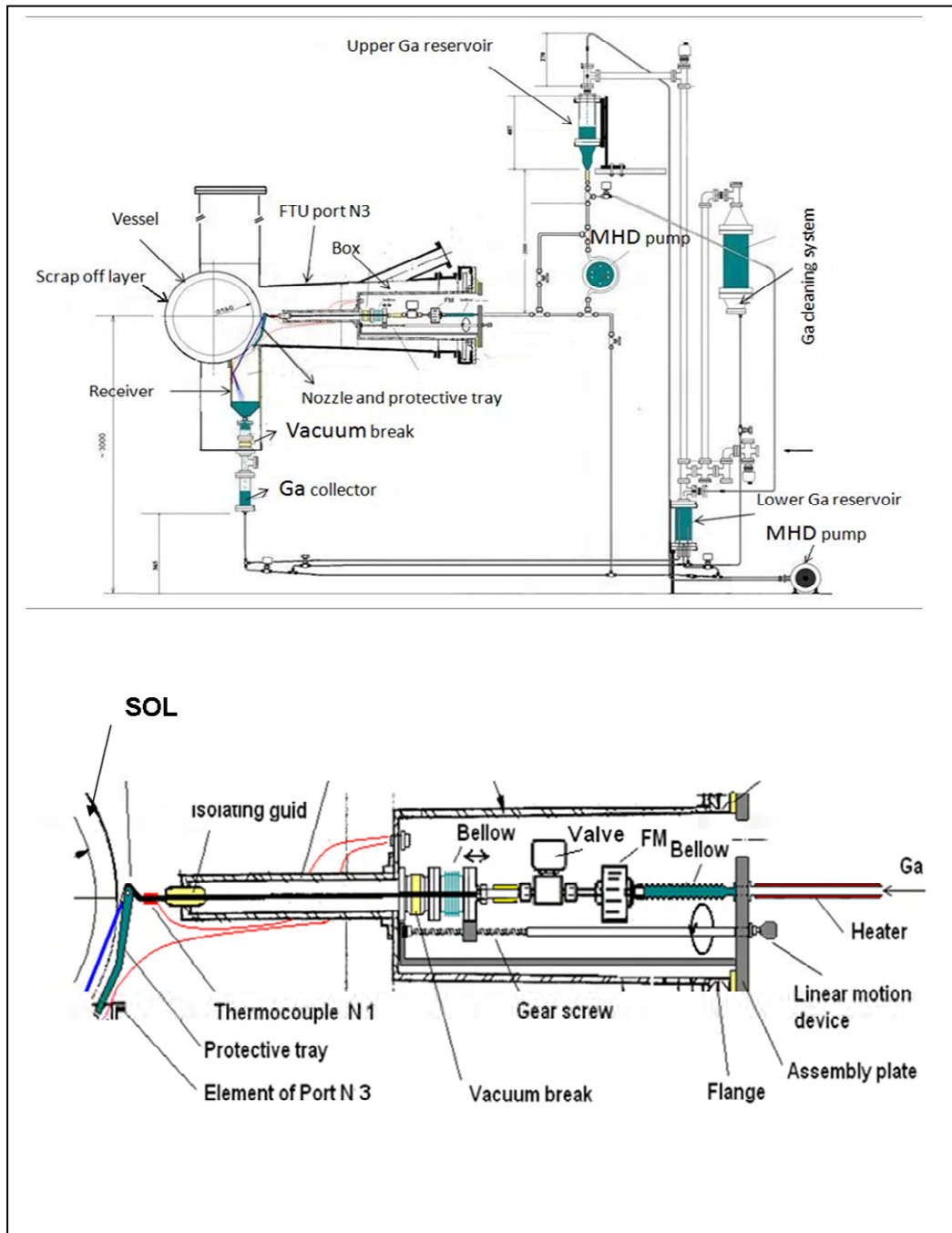


Figure 3.1.1. top - design proposal for MHD loop for Ga jet feeding; bottom - design of the module injector entry to port N3 of FTU.

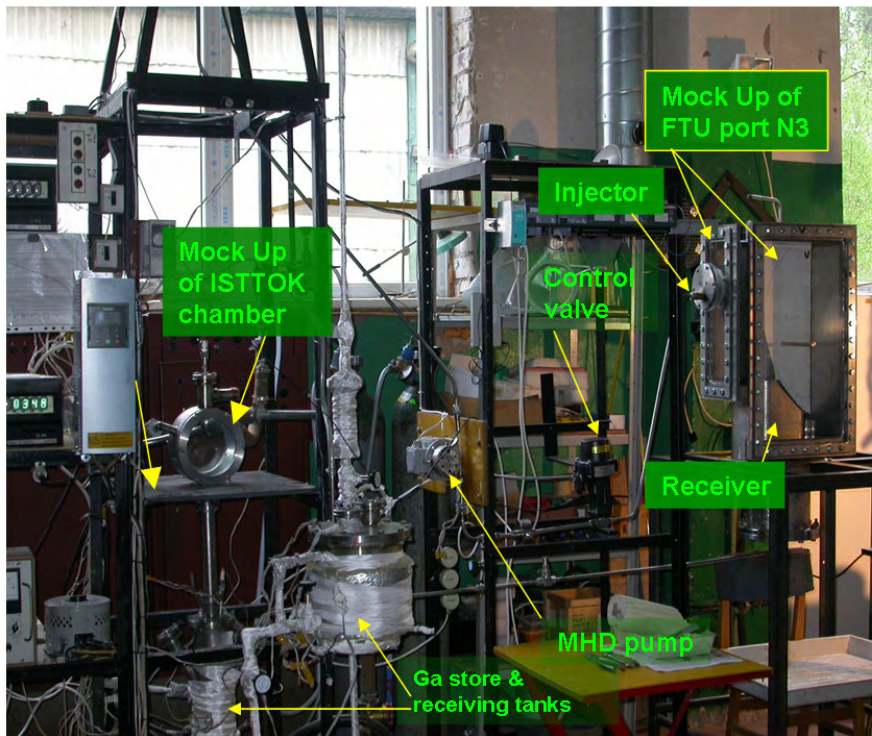
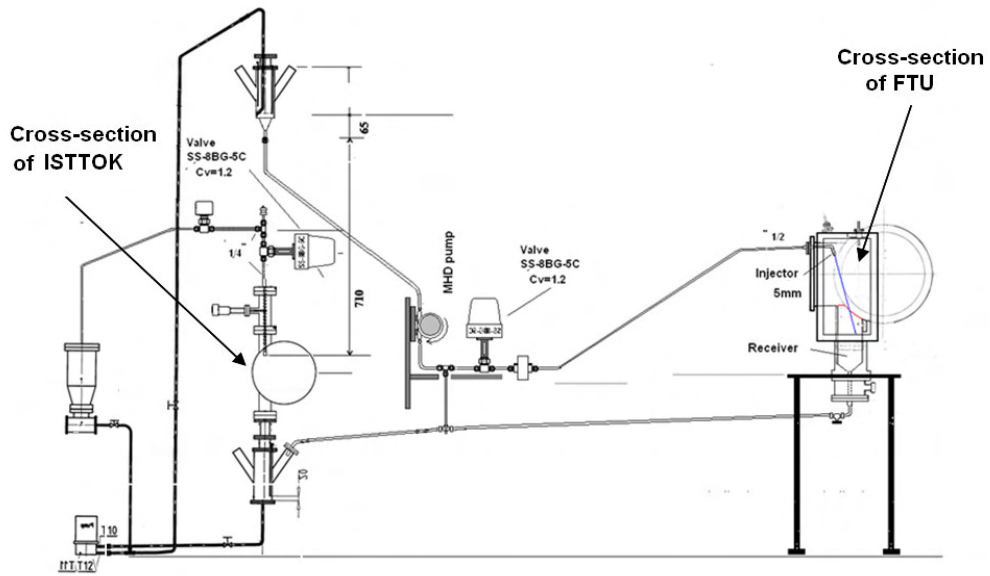


Figure 3.1.2. Upgraded In-Ga-Sn stands for investigation of free jets: top - scheme; bottom - photo.

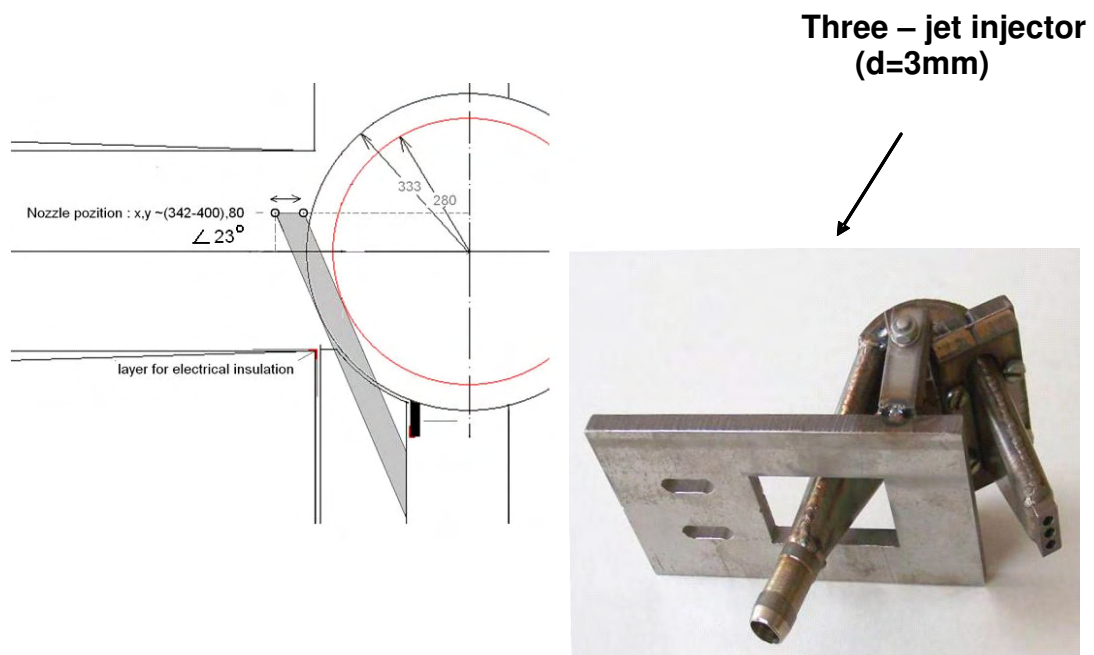
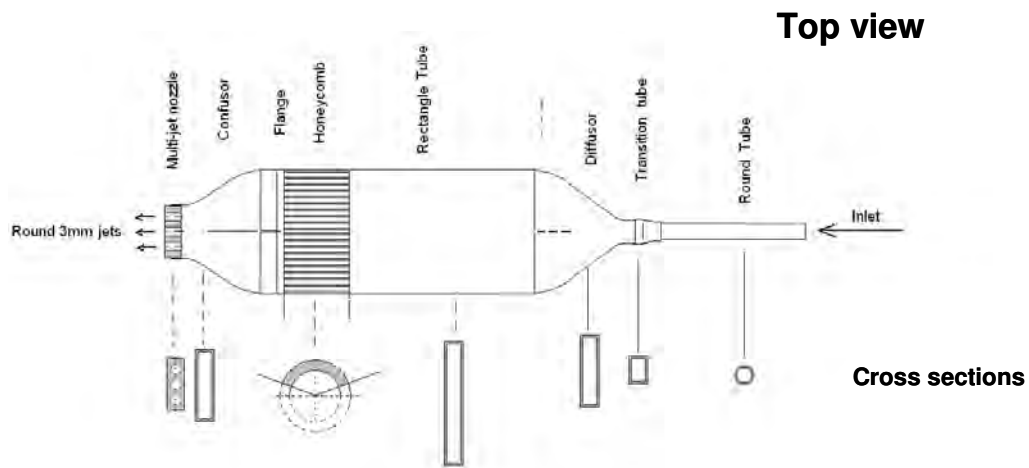
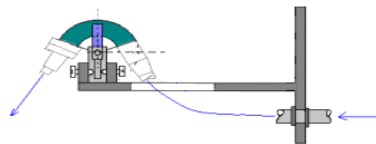


Figure 3.1.3. Scheme and mock-ups of region of jet's entry and three-jet injector.

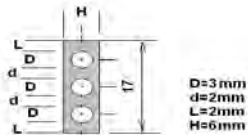
Three - jet injector



Side view



Flexible tube connection



Three jets nozzle dimensions

assembling flange

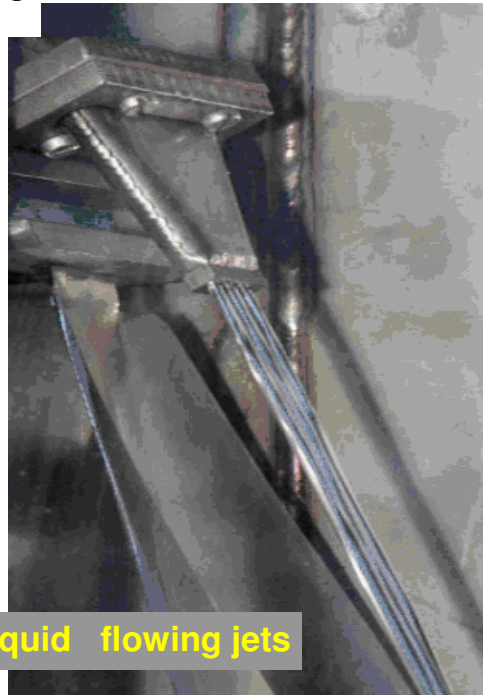


Figure 3.1.4. Design of three jet's injector; assembling and photo of injector at operation.

Reference

1. R.B.Gomes, H.Fernandes, C.Silva, A.Sarakovskis, T.Pereira, J.Figueiredo, B.Carvalho, A.Soares, P.Duarte, C.Varandas, O.Lielausis, A.Klyukin, E.Platacis, I.Tale, A. Alekseyv 'Liquid gallium jet-plasma interaction studies in ISTTOK tokamak', Journal of Nuclear Materials 390-391 (2009) 938-941.

3.2. Characterization of the impurity concentration, profiling and erosion in ITER relevant materials

WP09-PWI-01-02/UL/PS/BS

Principal investigator: I.Tale

LIBS spectroscopy of the impurity concentration depth profile in wall tiles

1. Background

Retention of tritium in the plasma facing components (PFC) will play an important role for the foreseen operation of ITER. Tritium will accumulate in the PFC as a result of gas dissolution, surface bombardment with T^+ , nuclear reactions of beryllium with neutrons, as a formation of a deposited layer etc. Distribution of tritium in a plasma chamber is asymmetric; tritium is mainly accumulated on the colder parts of the surfaces of the plasma chamber. Tritium inventory in the PFC is a real issue for safety concerns regarding future fusion machines or reactors. Tritium localization in PFC of ITER may cause tritium losses in the fuel. It is necessary to give assessment of the tritium retention in order to avoid too frequent stops of the machine for specific operations aiming at the reduction of the in-vessel inventory of tritium – i.e. for detritiation.

Because of the ability of carbon to withstand high heat flux and its favourable thermomechanical properties, carbon based tiles have been widely used for the first wall of the ASDEX and are the candidate material for the lower vertical targets of the divertor plates of ITER. The erosion of the carbon of the first wall by D-T plasmas leads to a co-deposition of hydrogenated carbon films mainly on the colder parts of the surfaces of the plasma chamber because of a high affinity of carbon to hydrogen isotopes. The formation of such co-deposited tritiated layers constitutes a major issue for ITER as it will tend to increase the tritium inventory trapped inside the fusion machine. Beryllium is also subjected to significant erosion under plasma-operating conditions; therefore a mixed Be-C film may be formed. Tritium depth profiles reported in literature revealed that a large fraction of the total tritium retained by a tile >61% had diffused deep into the bulk of the tile.

The coring/full combustion technique is mostly used in literature for determination of tritium depth profiles.

The alternative method for the impurity concentration profiling in solid materials is based on the laser ablation of material. Two quantities are available for impurity analysis in this case: fluorescence spectroscopy (LIBS) and mass spectroscopy (SIMS). The mass spectroscopy allows separating H, D and T isotopes, however, the sensitivity of traditional SIMS systems is low and available only in *ex situ* characterization of the plasma facing material (PFM).

Laser-induced breakdown spectroscopy (LIBS), being based on fluorescence measurements, allows to reach the principal limit of sensitivity. The main additional advantages of the LIBS for impurity analysis are simplicity, ability for detection of the trace impurity elements, corrosion of the layered tiles. LIBS offers a feasibility to perform the characterization of material at a distance.

During 2007 – 2008, the setup of laser ablation spectroscopy in the Institute of Solid State physics has been installed. The setup consists of a high energy sub-nanosecond pulse Nd:YAG laser, the data acquisition system based on the CCD camera for emission spectra acquisition, and high vacuum chamber equipped by two coordinate scanning stages. The ICCD detector and equipment for double-pulse laser ablation plasma heating is used to enhance the sensitivity of impurity detection up to the single photon events.

For development of the ITER-relevant *in situ* LIBS, the characteristics both of the laser ablation and the plasma plume emission using external equipment related to the design of the vessel segment are necessary to investigate. The main problems arise due to rather long distance between the reactor wall and equipment for both the ablation and the registration of plasma emission spectra.

Two crucial tasks for development of *in situ* LIBS are as follows: the accuracy of focusing of the laser beam on the wall and the sensitivity of the ablation plasma emission. The latter requires developing a new improved ablation plasma spectroscopy system.

Use of the Intensified CCD camera, having extremely high quantum efficiency for registration of single photons instead of CCD, is necessary.

Application of additional synchronous heating of ablation plasma by the second high energy laser pulse will facilitate multiple excitations of impurity atoms emitted from the wall.

2. Setup for development of the advanced LIBS spectroscopy of impurity distribution in ITER-relevant materials

The principle of the advanced tile ablation LIBS spectroscopy system for measurements of concentration distribution of impurities is represented in Fig.3.2.2.1.

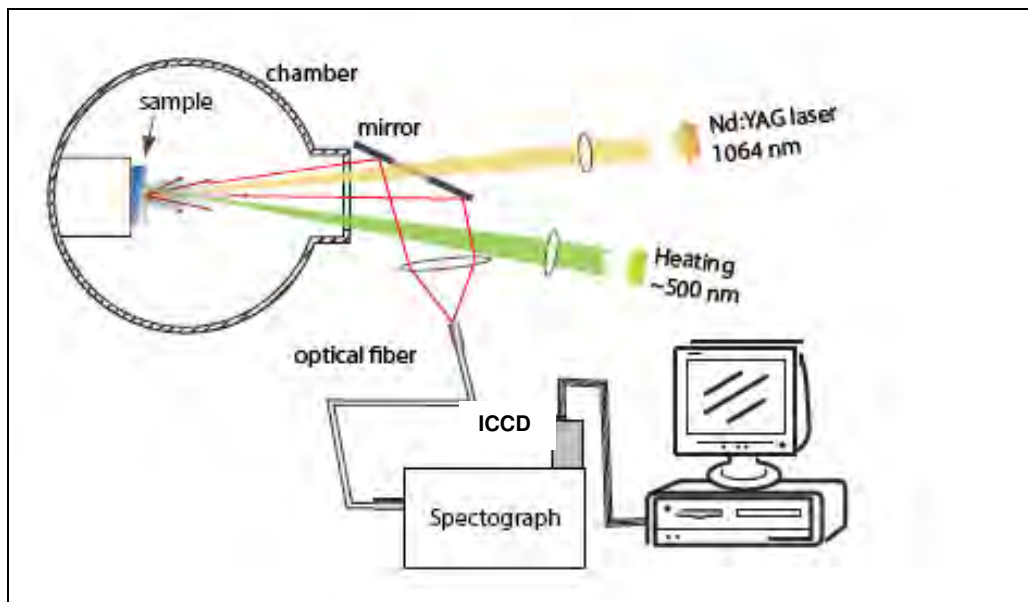


Figure 3.2.2.1. The principle of the advanced LIBS spectroscopy

The sample of reactor wall is placed in vacuum chamber equipped with an optical port. Through the window the sample is illuminated by focused Nd:YAG laser beam (1064 nm) pulse resulting in ablation of sample material and formation of plasma plume. The plasma plume is heated by the other defocused Nd:YAG laser pulse (~533 nm) with a given delay to enhance the ablation plasma emission. Plasma emission is collected through the optical port by objective lens, focused on the entry of optical fibre guiding emission beam to the remote spectrograph. The latter is equipped with the ICCD camera.

3. The functional setup of equipment

The functional setup for development of the *in situ* spectroscopy of impurity characteristics in plasma facing wall is shown in Fig. 3.2.3.1.

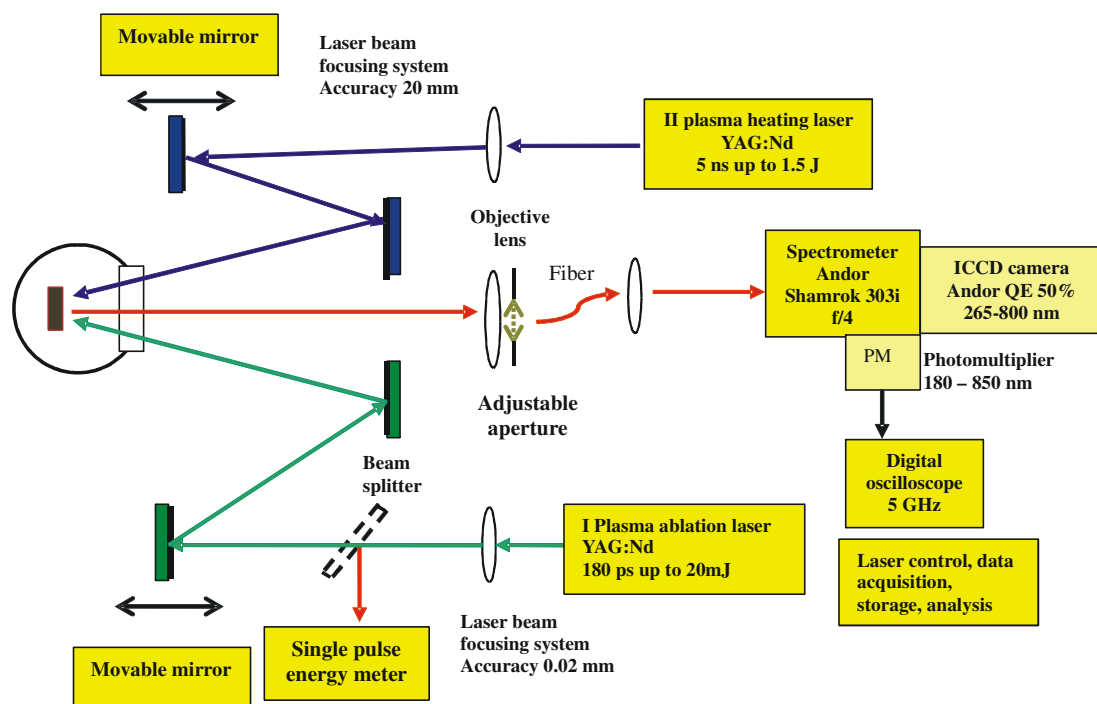


Figure 3.2.3.1. Setup of the equipment for development of *in situ* LIBS spectroscopy in the plasma facing wall of the reactor.

For *in situ* implementation of LIBS spectroscopy, only one common optical port is available to access the wall. The maximum aperture is defined by the diameter of the port. Directions of the laser beam and observation of the ablation plasma plume will be close to the wall normal plane.

4. Setup of the equipment

4.1 Setup of the ablation laser

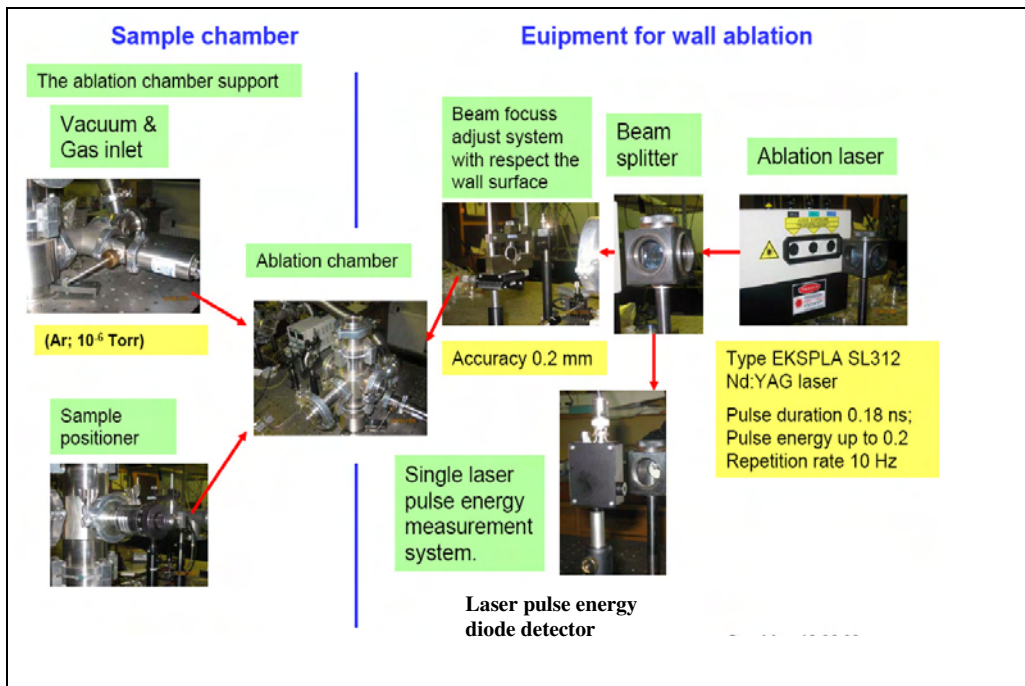


Figure 3.2.4.1. The vacuum chamber and equipment for ablation of the wall surface layer

Ablation of thin surface layer of the wall is provided by the first (I) Sub-nanosecond single pulse of Nd:YAG laser with pulse duration 180ps and variable pulse energy up to 20 mJ.

Laser beam is focused on the wall surface by adjustable lens system placed in front of the laser. The position of the focus plane on the wall surface is the crucial parameter of ablation process. It defines the diameter of the ablation crater and pulse intensity distribution on the wall surface.

The required beam focusing accuracy by the distance from the laser source to the wall up to about 10 m must be $\pm 0.2\text{mm}$.

For modelling the laser beam distance to the wall, a pair of optical mirrors with movable inter-mirror spacing is applied.

4.2 Single laser pulse energy detector

Using beam splitter, a part of the emission beam flux is directed to the detector of single pulse energy meter, which is necessary for correction of single laser pulse variation being up to 1% of the full energy value.

Type NOVA2 Ophir thermopile PE25BB detector has been applied for pulse energy measurements. The sensor characteristics are: aperture 25 mm, spectral region 0.15-20 μm , energy range 100 μJ - 10J, noise level 20 μJ . The control and acquisition of pulse energy data have been integrated in the LABVIEW equipment control system.

4.3. Setup of the plasma heating laser

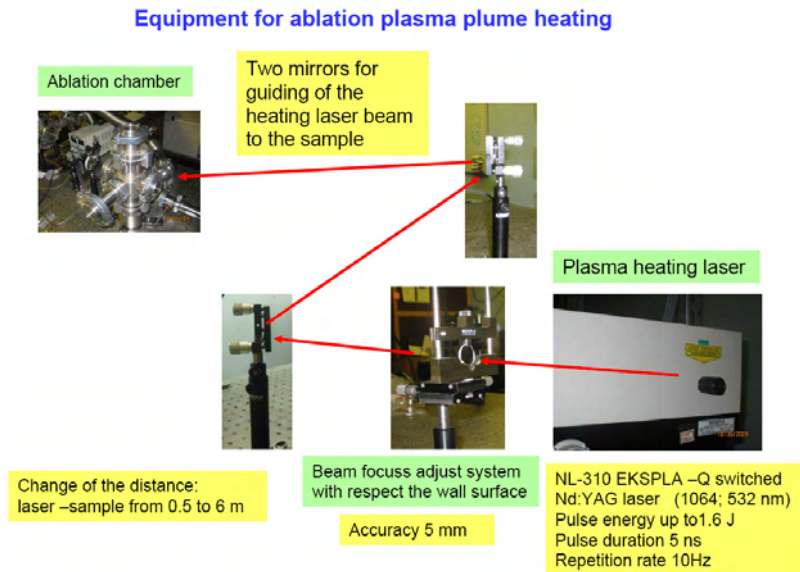


Figure 3.2.4.2. Equipment for the ablation plasma plume heating

Heating of the ablation plasma plume is provided by the second (II) heating Nd:YAG laser single pulse with pulse duration of 5-6 ns and variable energy up to 1.6 J at 1064 nm or 0.8 J at 532 nm. The laser pulse is focused by optical system to the diameter of 0.1 – 5 mm being close to the diameter of plasma plume. Similar pair of mirrors with movable inter-mirror spacing is applied for modelling of the laser – sample distance.

4.5. Setup of the plasma spectroscopy

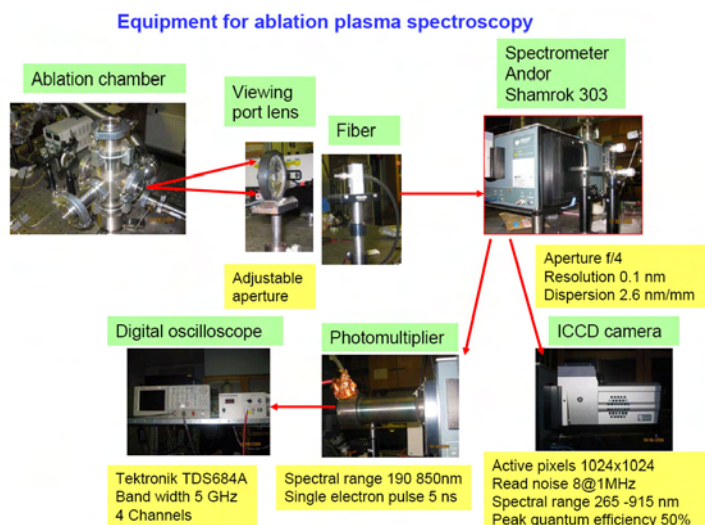


Figure 3.2.4.3. Equipment for spectroscopy of the wall ablation plasma

Equipment for emission spectra measurements of the ablation plasma plume contains the following functional parts.

The emission is collected by the objective lens which in the real *in situ* equipment will be mounted directly in the optical port. For modelling the light collection characteristics, the objective lens of the experimental laboratory setup has maximal aperture of f/4 corresponding to the aperture of the used spectrograph. Adjustable diaphragm in front of objective lens allows providing modelling the effective distance from the lens to the ablation plume. The emission beam is focused on the fibre bundle. At the entry end of the bundle two different single fibre configurations are applied: round and linear. The single fibre configuration at the output end is linear for focusing the emission beam on the spectrograph entry slit.

Technical characteristics of the ICCD camera ANDOR DH734-18F-A3.

Maximum photocathode quantum efficiency is 45%, the spectral range is 270- 810 nm, active pixels – 1024x1024, active area – 13.3x13.3 mm, system readout noise (at -20°C and minimum exposure time under dark conditions): typical at 1Mhz: 8 e⁻/pixel, maximum at 1Mhz: 16 e⁻/pixel.

The ICCD camera is equipped with programmable gate pulse delay and width from 0 ns to 25 ms (resolution 25 ps).

The programmable gate pulse delay and width system enables to perform the spectra acquisition in a time window delayed with respect to the ablation laser pulse and/or plasma heating pulse, thus optimizing the emission readout with respect to the decay characteristics of plasma thermal emission.

An additional equipment for measurements of the decay kinetics of a single emission line (e.g., D_α) has been implemented. Separated by the exit slit of a spectrograph, the emission line of an element has been detected by the photomultiplier tube (spectral region 180 – 900 nm) connected to the digital averaging oscilloscope.

The control of the ablation laser, the plasma heating laser, the laser pulse energy meter and the equipment for plasma emission spectroscopy, including spectrograph and ICCD camera, have been performed using LABVIEW computer program. The data acquisition massive for each laser pulse contains plasma emission spectrum, ablation laser power, time and ICCD gate delay parameters.

5. Development of the advanced LIBS technique for the impurity distribution analysis in ITER-relevant materials

5.1 Sample preparation

Three types of tile materials have been used for investigation:

1. Graphite R6710 tile #1 for reference studies
2. AUG post mortem graphite:
 - Tile #2.1 Experiments from year 2003
 - Tile #2.2 Divi.o., x/6/8, D2, 2003
3. AUG post mortem W-coated graphite:

Tile #3 HS, C4, S14, 2002

Samples for the investigations have been cleaved out from tiles.

Sample dimensions of tiles #1, #2.2, #3 - 20x20x6 mm

Sample dimensions of tile #2.1 - Φ 20x6 mm.

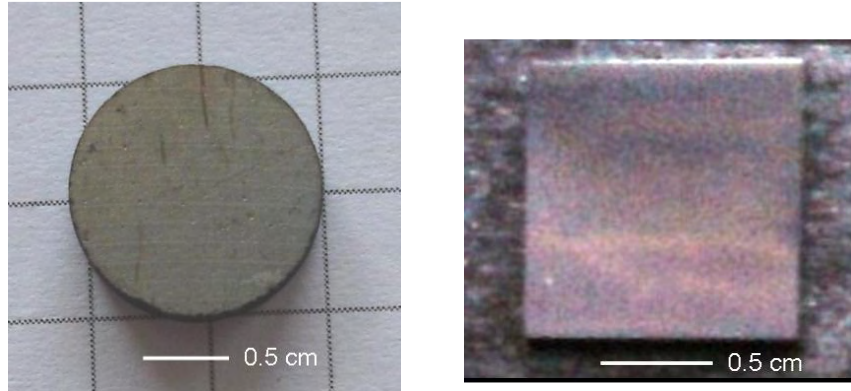


Figure 3.2.5.1. Round and rectangular samples cleaved from AUG tiles

For investigations in vacuum at different pressures, the samples were placed on the rectangular sample holder and fixed by a spring (Fig. 3.2.5.2). The sample holder was mounted to the rotating feed through and inserted into the vacuum chamber. It can be also modified to use round samples. They were inserted into the stainless steel ring and placed in the holder.

Laser beam was focused onto sample at ~6 mm from the holder rotation centre. To perform an ablation at the different parts of sample, the position of the laser spot on the target has been changed by turning the sample holder.

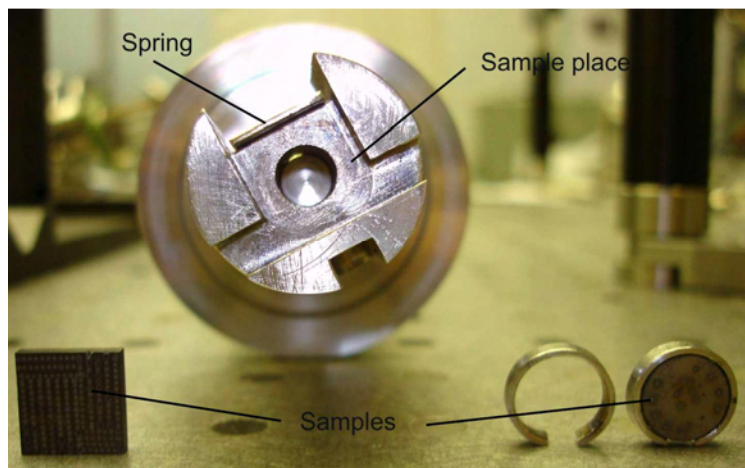


Figure 3.2.5.2 Sample holder for experiments in vacuum and low pressures

For investigation in air samples were fixed at XYZ translation stage.

A number of ablation experiments have been performed using single sample. Fig.3.2.5.2 represents both the rectangular sample investigated in air using XYZ translation stage and the round sample investigated in vacuum chamber and positioned by sample rotation.

Fig. 3.2.5.3 shows SEM image of the surface of graphite sample #2.1 after ablation experiments.

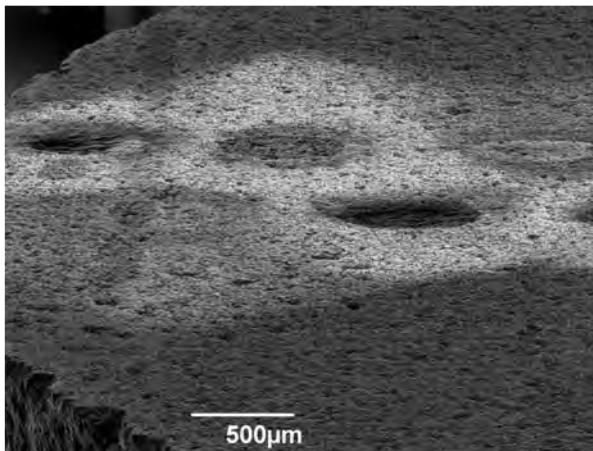


Figure 3.2.5.3. SEM image of an ablated target #2.1

5.2 Laser beam setting and optimization of crater formation

The characteristics of the laser beam for impurity profiling is a task of a crucial importance. Apart from the laser beam wavelength and duration, formation of the ablation crater is affected by the shape of the laser beam and the density of pulse energy. Stability of pulse-by-pulse emission is very important for characterisation of impurity depth profile.

Laser source for LIBS spectroscopy of impurity depth profiles in PFCs used in the investigation have been optimized regarding to the pulse duration, pulse repetition rate and pulse energy. The Nd:YAG EKSPLA SL312 laser has pulse energy up to 250 mJ at 1064 nm, 120 mJ at 534 nm and 80 mJ at 354 nm, repetition rate is 10 Hz. Electro-optically Q-switched and temporally compressed by backward stimulated Brillouin scattering (SBS), lasers serves as an excellent solution for the applications requiring high energy sub-nanosecond pulses of 150 ± 20 ps.

Application of the sub-nanosecond pulses instead of typical Q-switched Nd:YAG lasers considerably diminishes the thickness of a layer removed with the single pulse down to ~ 100 nm.

○ Laser beam characteristics

The photography of the adjusted laser pulse is represented in Fig. 3.2.5.4

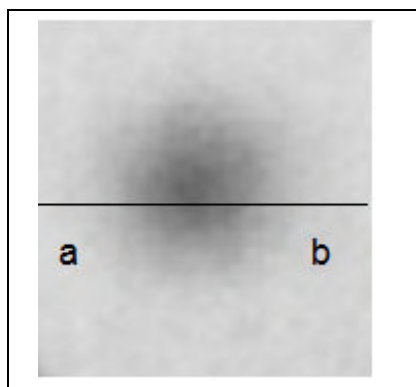


Figure 3.2.5.4. A photograph of the single shot of the laser SL312 beam at 1064 nm, 100 mJ

The maximum intensity fits the centre of a beam. The intensity distribution in the both direction a-b and in the perpendicular one is slightly asymmetric. The corresponding distribution obtained by the analysis of the photography is represented in Fig.3.2.5.5.

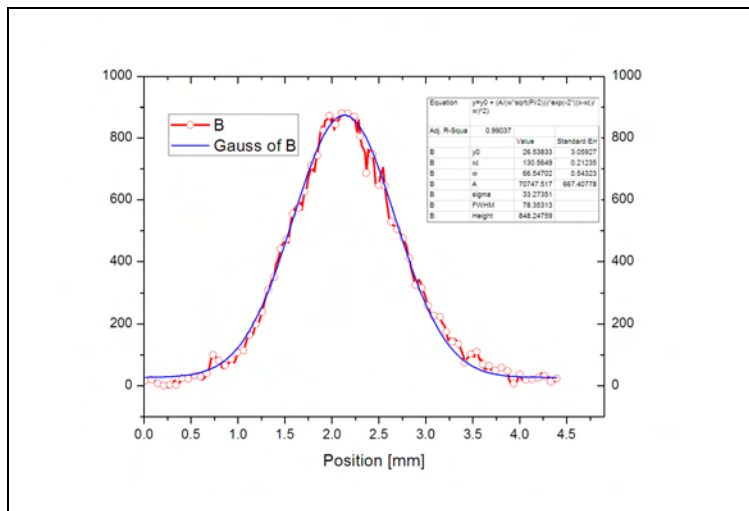


Figure 3.2.5.5. Intensity distribution of the laser pulse calculated by analysis of the photography along the line a-b (see Fig. 3.2.5.4)

The intensity distribution is close to the Gauss curve. The deviation of the intensity distribution occurs only at the wings.

It can be concluded that the features of the ablation crater formation are caused by the peculiarities of the light interaction with the material.

Investigation results of the dispersion of laser pulse energy are represented in Fig.3.2.5.6.

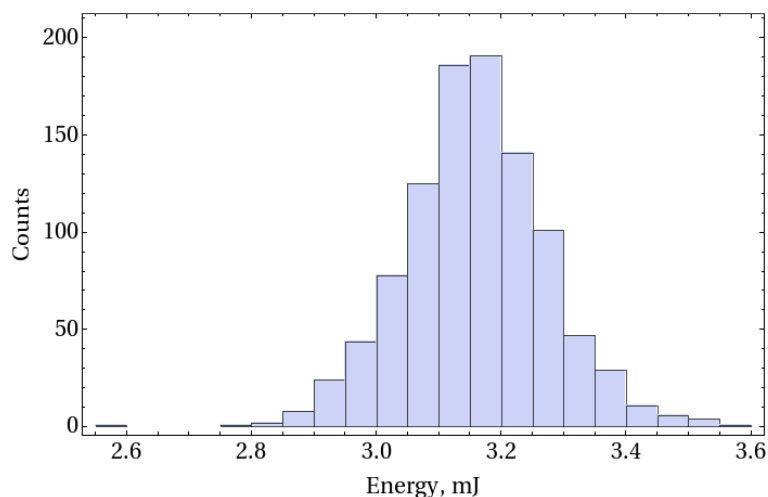


Figure 3.2.5.6. Histogram of the pulse energy distribution for laser SL312 measured at the wavelength of 1064 nm and pulse energy of 3.15 mJ

The shape of the pulse energy distribution nearly corresponds to the Gauss distribution function. The mean square deviation is 3.15 ± 0.1 mJ. Like the intensity distribution, the pulse energy distribution is slightly asymmetric. It should be pointed out that in addition to the main distribution of pulse energy, a pulse characterized by considerably smaller energy at about 2.58 mJ occurs. Low energy pulses are randomly distributed in the series of 3.15 mJ pulses. The mean repetition rate of low energy pulse is about 1 per 20 pulses of average energy.

Conclusion: the energy measurements of single pulses are necessary to include in the LIBS spectroscopy methodology for correction of the dispersion of single pulses as well as for elimination of low energy pulses in calculation of ablation crater depth.

○ Ablation crater formation

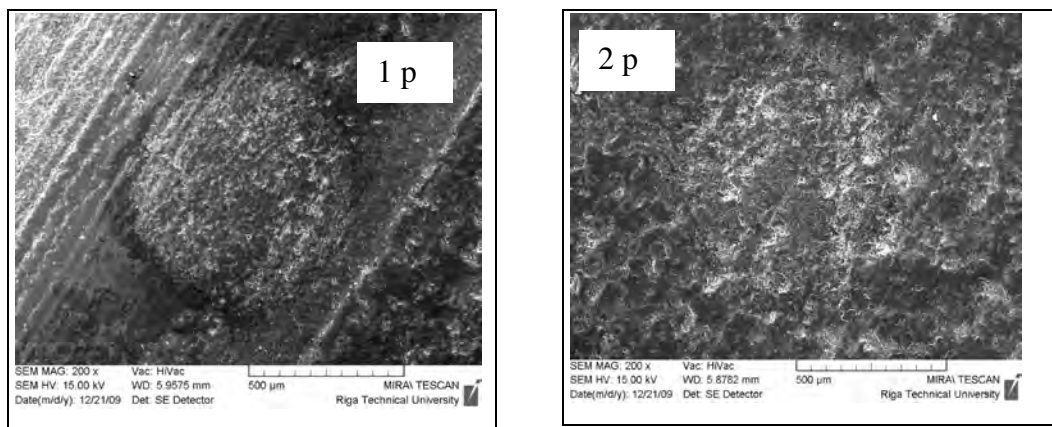
The initial stages of the crater formation were investigated using scanning electron microscope (SEM) imaging of the sample before interaction with laser and in the course of ablation events starting from single pulse.

The formation of ablation crater at high number of single events was investigated using Dektak 150 profiler. Measurements are taken electromechanically by moving the sample beneath a diamond-tipper stylus. The high-precision stage moves a sample according to a user-programmed scan length, speed and stylus force. The stylus is mechanically coupled to the core of a linear variable differential transformer. The transformer scales as an AC reference signal proportional to the position change, which in turn is converted to a digital form.

Investigations of the first stages of crater formation were performed for the post-mortem graphite, sample # 2.2 and W-coated graphite, sample #3.

Ablation by different number of laser shots was made in neighbouring positions of a single sample, which was placed in vacuum. Thus, the present SEM measurements do not contain information about the evaluation of the local structure of the surface after each laser shot. The surface images represent the formation features of the whole laser ablation crater.

Fig. 3.2.5.7 show the crater evaluation for graphite sample #2.2 by using 6 mJ energy pulses, Fig. 3.2.5.8 – using 15 mJ pulses.



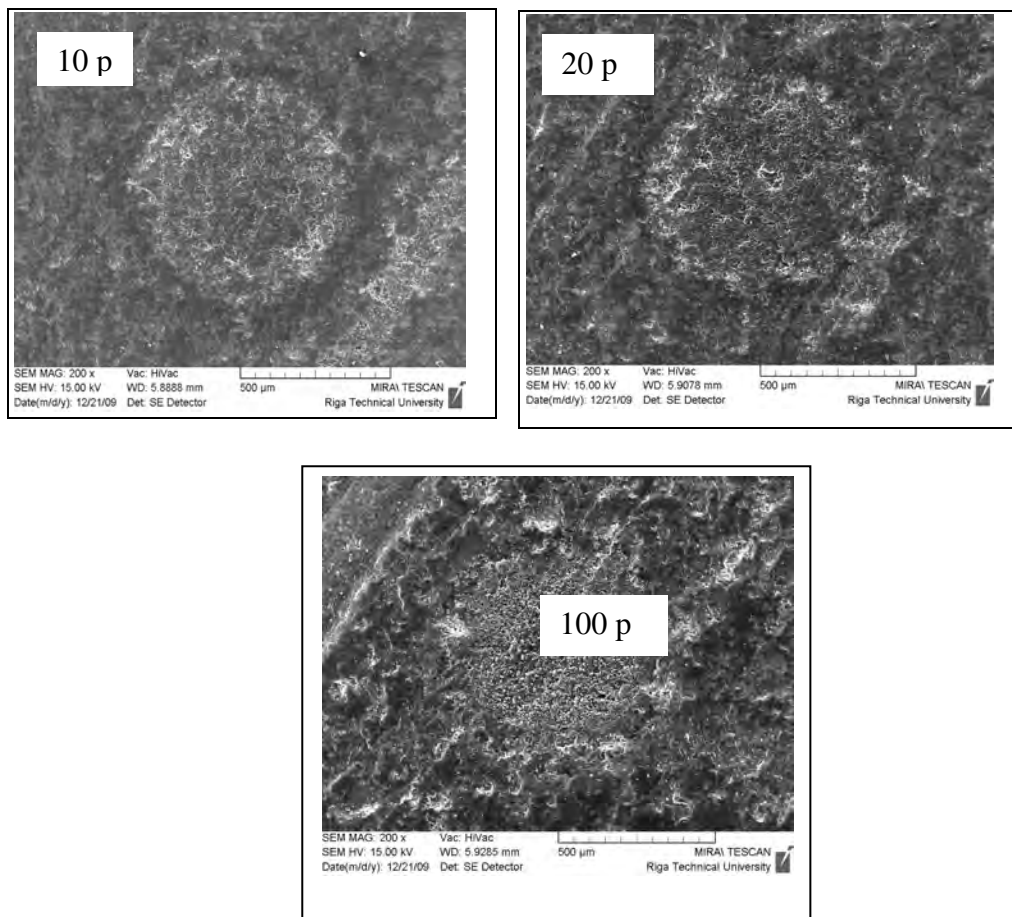


Figure 3.2.5.7. Sample #2.2: SEM images of a surface exposed by 6 mJ laser pulses;
pulse energy density – 1.2 J/cm^2 ,
pulse power density – $8 \times 10^9 \text{ W/cm}^2$

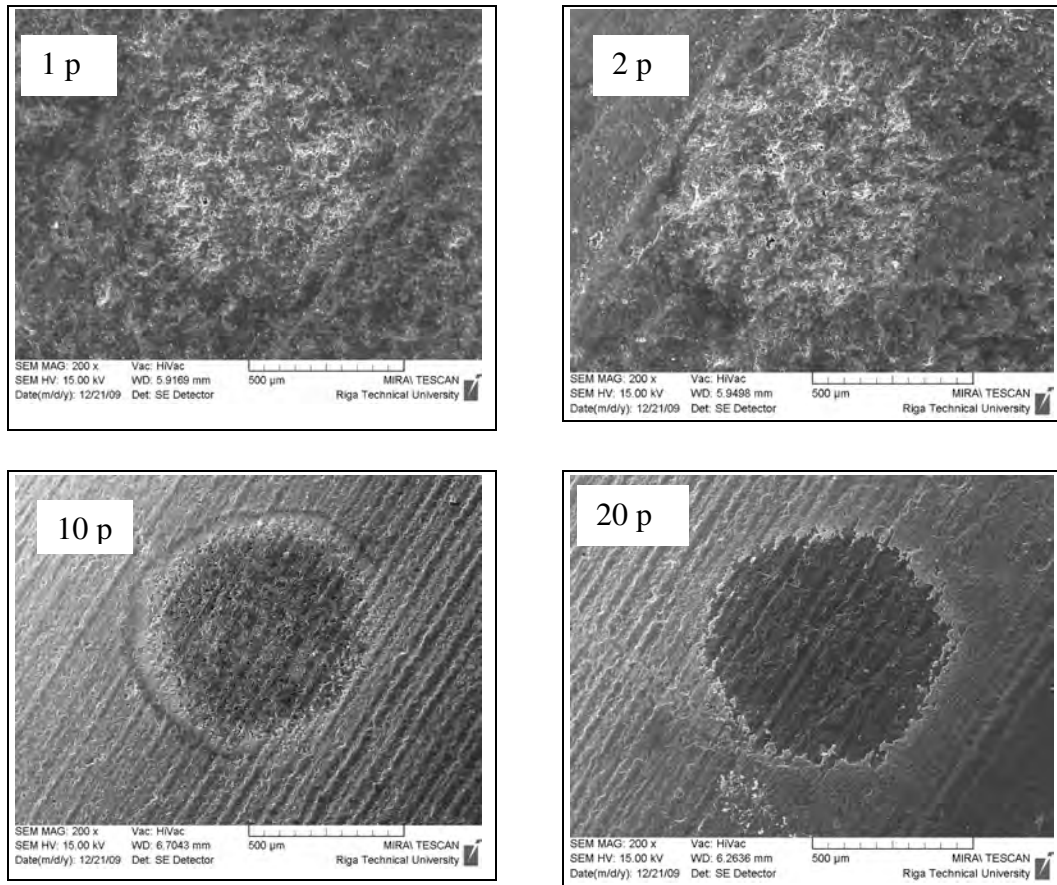


Figure 3.2.5.8. Sample #2.2: SEM images of a surface exposed by 6 mJ laser pulses.

Crater diameter $\approx 800 \mu\text{m}$, pulse energy density – 3.0 J/cm^2 , pulse power density – $2.3 \times 10^{10} \text{ W/cm}^2$

SEM images show the topography of an electron backscattering from the sample surface. The backscattering intensity reflects the efficiency of the secondary electron emission depending on the material and charge state of surface. For metals, the probability to emit secondary electrons considerably exceeds that of semiconductor materials and increases for high Z metals. The surface of insulators is negatively charged, which results in the increased scattering of primary electrons.

Investigated graphite samples do not contain metal inclusions. Bright regions correspond either to the insulating material or to the particles charged due to the absence of electric contact with the sample.

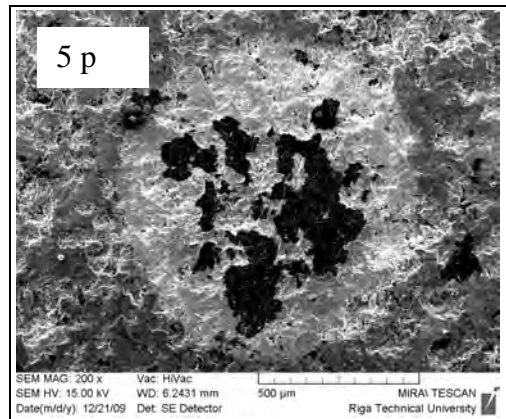
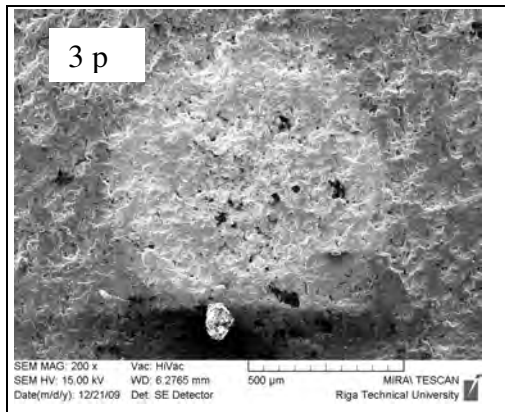
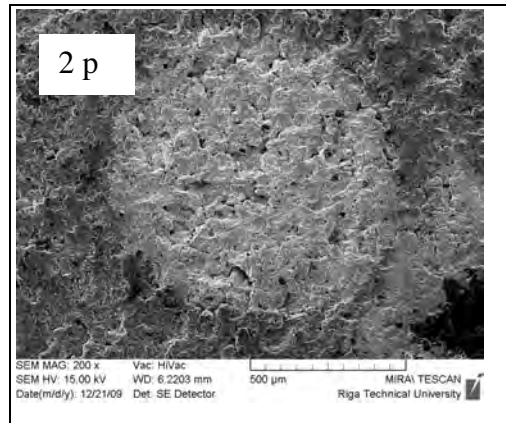
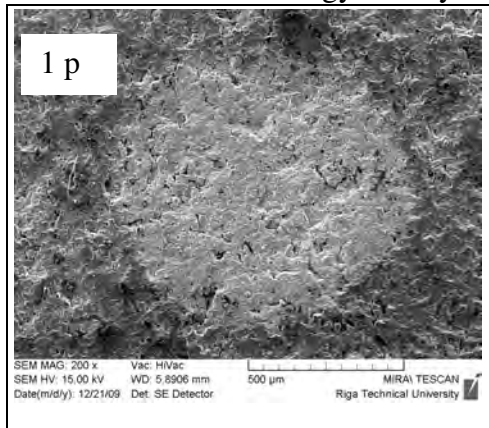
After the single shot (Fig 3.2.5.7, 1p), the ablated region is clearly pronounced. Surrounded by a dark ring, it contains multiple bright spots. The structure of the

bright regions is similar to the initial surface structure of the sample (Fig. 3.2.5.7, 2p, 10p, 20p). The results indicate that the dark ring corresponds to the formation of vertical crater wall even starting with the first shots.

The interaction of intense light pulse with the surface together with formation of plasma results in development of dust particles on the surface of material. They are represented by the bright spots. The dimension of the dust particles decreases with the increase of the crater depth (Fig. 3.2.5.7, 100p).

Similar results have been obtained when the pulse energy was increased up to 6.5 mJ. The diameter of crater remains unchanged. The preventable dust particle creation is restricted only by few shots at the beginning. The bottom of the crater replicates the initial structure of the material (Fig. 3.2.5.8, 20p).

In conclusion, the pulse energy density has crucial influence on the ablation process. The high regularity of the thickness of the ablated layer can be reached when a definite limit of the energy density is exceeded.



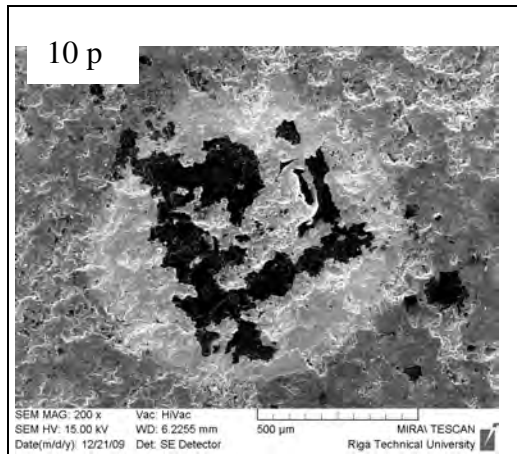


Figure 3.2.5.9. Sample #3: SEM images of a surface exposed by 6 mJ laser pulses; pulse energy density – 1.2 J/cm^2 , pulse power density – $8 \times 10^9 \text{ W/cm}^2$

SEM images of the W-coated graphite sample are represented in Fig. 3.2.5.9. The first shot results in formation of a surface characterized by high average brightness. The structure of ablated surface part remains the same as the initial one. A number of brighter spots are present. We assume that the first shot exposes W layer with dust particles on it. The 3rd shot results in creation of the dark spots. They are expanded by the next shots indicating that the part of the W-layer is removed from the sample.

The direct shape of the ablation crater at high number of pulses as well as the ablation rate at different laser pulse energy have been examined by the profiler.

Figure 3.2.10 represents pits of relevant pulse energies obtained for 100 pulses.

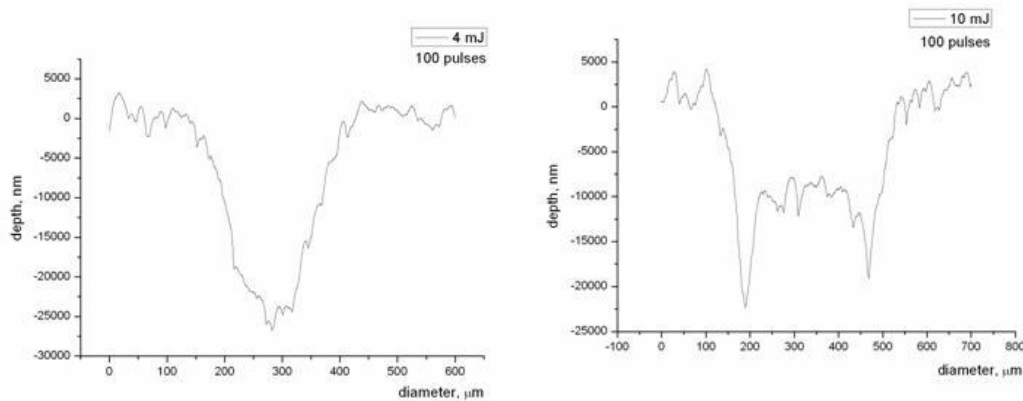


Figure 3.2.5.10. The depth profiles of the crater obtained at different laser pulse energies obtained for 100 shots: left – 3mJ, right – 10 mJ.

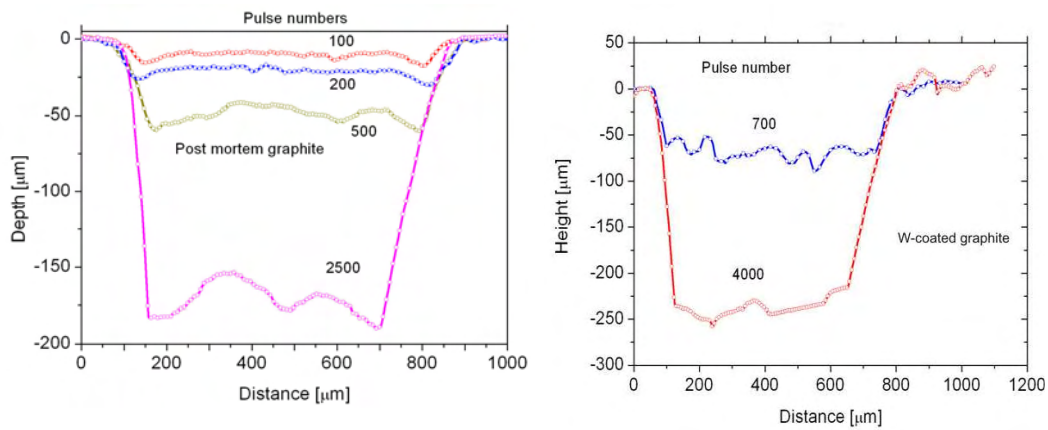


Figure 3.2.5.11. The depth profiles of the crater obtained at different number of laser shots at pulse energy 10 mJ: Left: sample #2.2; right sample #3.

At high intensities of the incident laser beam, one can notice a specific track around the edge of the ablation crater. We expect that this is result of edge diffraction occurring during the ablation process.

5.3 Plasma plume spectra measurements and line analysis

- **Plasma emission lines in the carbon tiles for H,D,T LIBS**

The concentration profiles of hydrogen isotopes D and T are of the main interest in analysis of the impurities in wall tiles. In the visible spectral region available for *in situ* analysis of the wall tiles, three D lines are present. The main emission line is of the highest intensity.

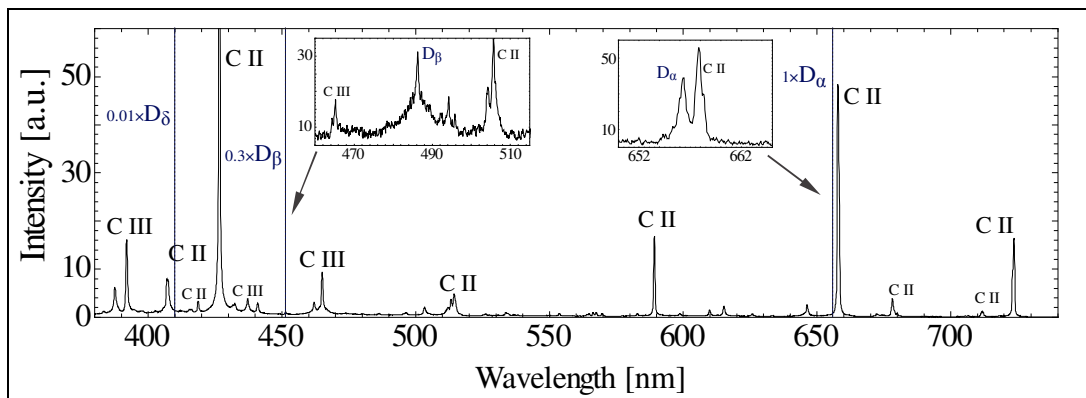


Figure 3.2.5.12. The D_α , D_β and D_γ spectral lines in the carbon tile #2.1

D_α overlaps with the carbon C_{II} emission line. To determine the line intensity, spectral measurements with corresponding resolution followed by line fitting procedure have

to be applied. The intensity of the single D_{β} emission line is about of 3 times less with respect to the D_{α} line and can be applied for concentration analysis.

- **Emission spectra in the different positions of plasma**
 - **Side observations of the plume spectra**

The image of plasma plume has been reproduced by convex quartz lens, thus by shifting the optical fibre at position S_2 point of lens it is possible to measure the spectral contents of plume at different positions (Fig. 3.2.18).

$$\frac{1}{S_1} + \frac{1}{S_2} = \frac{1}{f}$$

Due to the weak signal, the averaging of 100 images has been applied at each position. Therefore the spectra contain averaged information on element concentration within the depth of at least 1 mm.

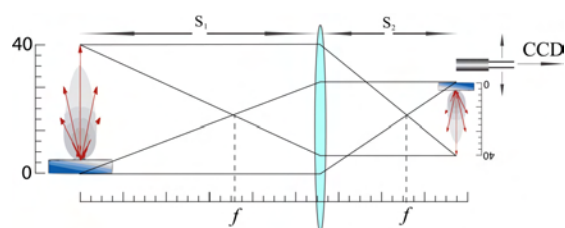


Figure 3.2.5.13. Plasma plume scanning

Obtained spectra are shown in Figure 5.14. Note that the correction for sensitivity of CCD camera for following images has not been applied.

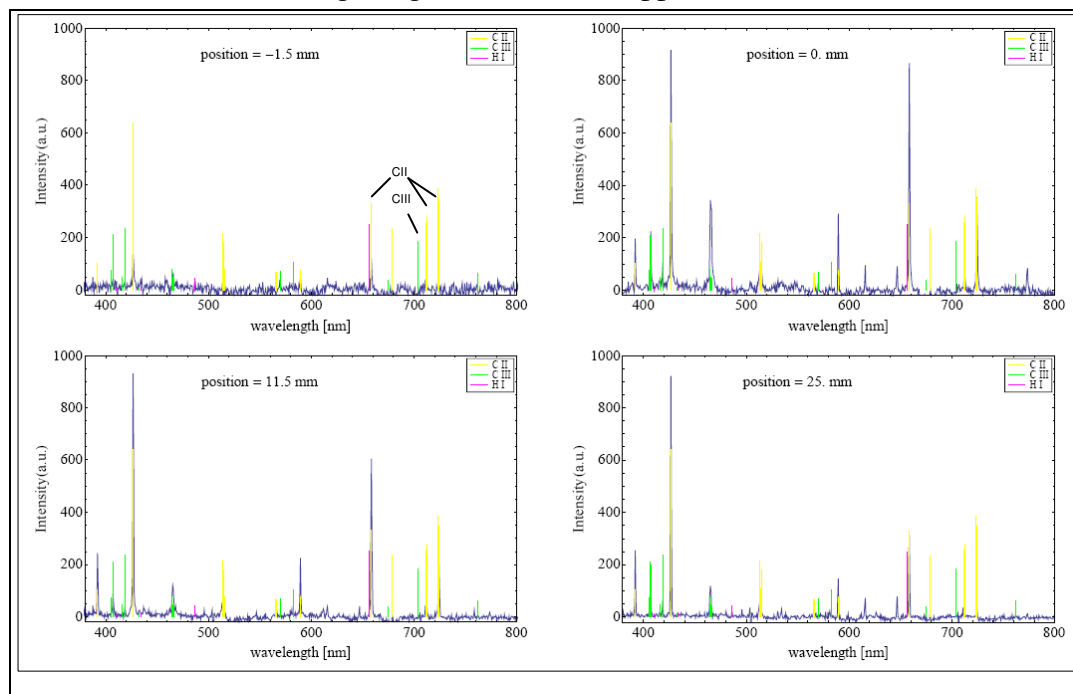


Figure 3.2.5.14. Spectra of laser induced plasma plume at different positions

The first image (Fig. 3.2.5.14, top left) is acquired at the position outside the generated plasma, but still some spectral lines can be found due to the scattered light.

The slight differences in intensities of spectral lines in the following images appear only due to the fluctuations of the laser output power and also due to the lack of synchronization, when the delay between the irradiation and the signal detection is not well defined. Note that the H I lines appear only within first 5 impulses, therefore, they are not visible in the spectra images in Figure 3.2.5.14.

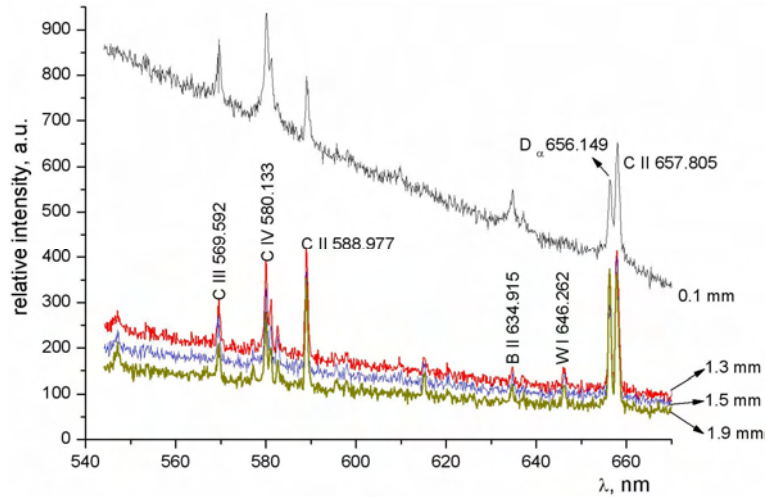


Figure 3.2.5.15. Spectra of laser induced plasma plume at different positions at atmosphere pressure. Sample #2.1.

At atmosphere pressures the plasma plume expands only over a few cm. Strong background arising from continuous thermal radiation appears close to the tile surface. Emission lines of carbon D, B and W are broadened.

Results indicate that by increase of the gas pressure the emission of the laser induced plasma plume becomes suppressed in small volume close to the target. High gas pressure supports providing LIBS spectroscopy perpendicular to the plasma expansion direction. However, the spectra are affected by strong thermal background emission.

○ **Frontal observations of the spectra of the plume**

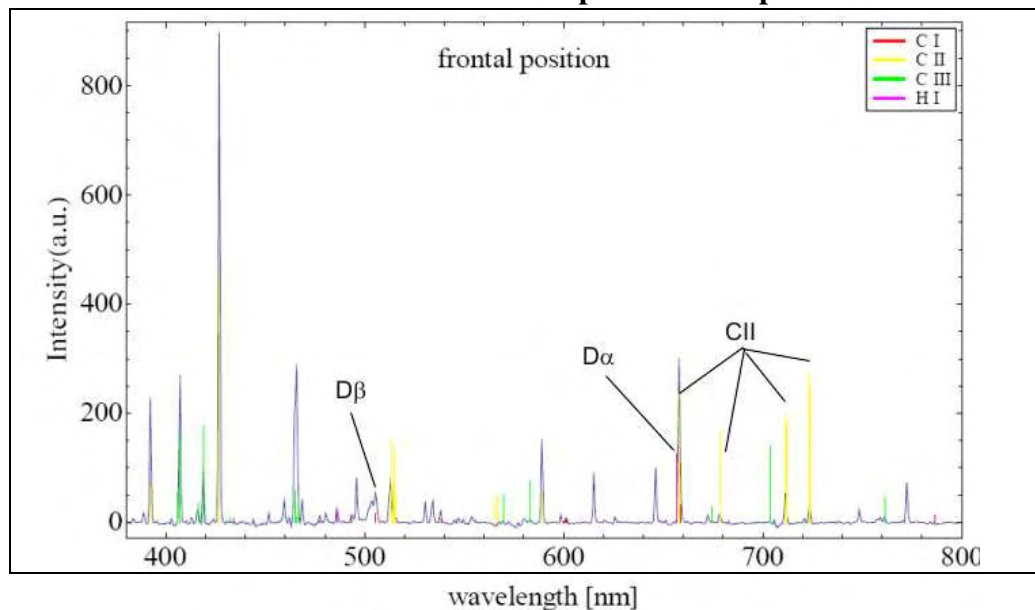


Figure 3.2.5.16. Spectra of laser induced plasma plume acquired from the frontal position in vacuum, sample #2.1

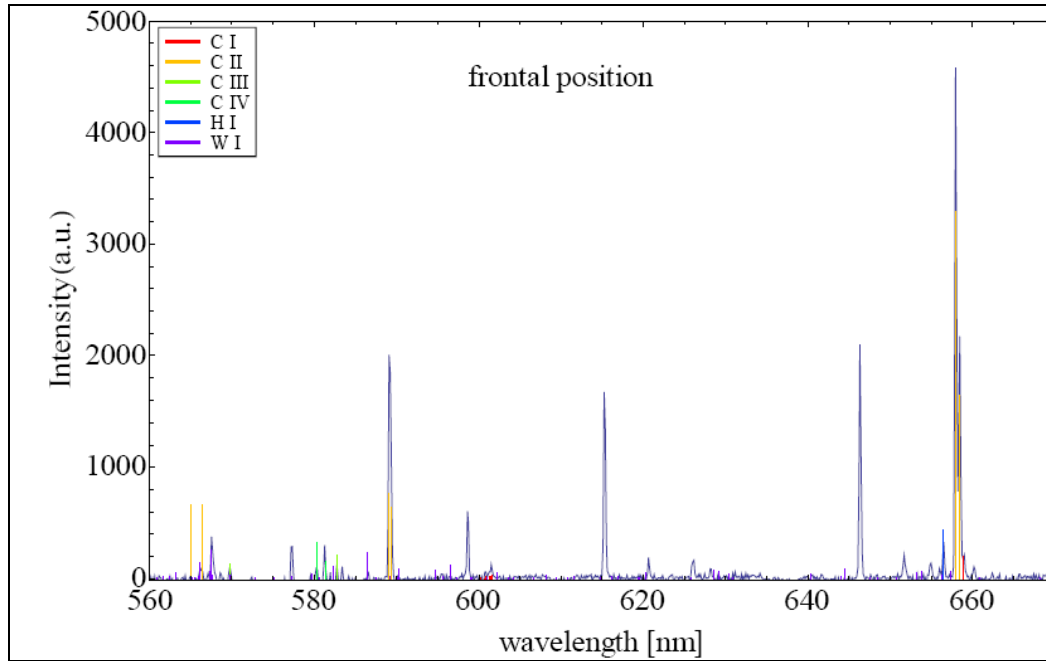


Figure 3.2.5.17. Spectra acquired from the frontal position with higher resolution

At higher resolution, an H I (656.5 nm) spectral line can be distinguished, so also looking from this position the spectral line is visible. Note that the origins of intense 615.3 nm, 646.35 nm and several weaker lines have not yet been found.

In general, the spectral composition of the detected light coming from the frontal window has not been changed (see Fig. 3.2.5.14). Only due to the partial light collection the total light intensity is lower compared to the case when acquired from the side window. But in this case signal to noise ratio is better because of increased number of averaging. That can be corrected by applying a mirror with a hole in the middle allowing laser beam to pass through.

6. Impurity depth profile analysis

To record the spectral information and depth profiling of the impurities in the ASDEX Upgrade samples – deuterium and boron – a consecutive laser pulses have been applied to the same spot of target. The spectra were recorded during each applied pulse. As a result, each set of spectra comprises as many spectra as the number of pulses.

- **Post-mortem analysis of carbon plates from ASDEX**

- **Carbon tile #2.1**

For investigation of the feasibility of LIBS spectroscopy in impurity depth profile determination, four laser pulse energies have been used ranging from 2 mJ to 5mJ.

The spectra are shown in Figures 3.2.6.1, a-d.

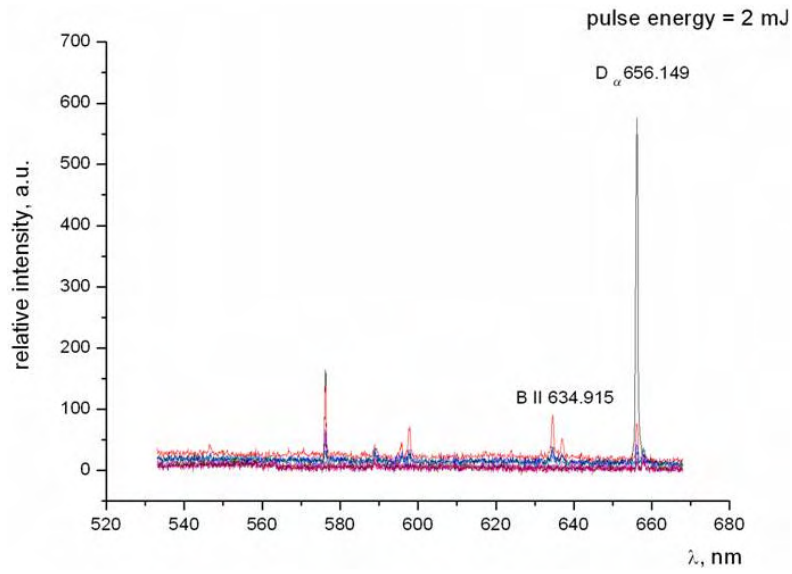


Figure 3.2.6.1, a: The spectra after 9 consecutive pulses. Evaluation of the deuterium versus boron and carbon lines

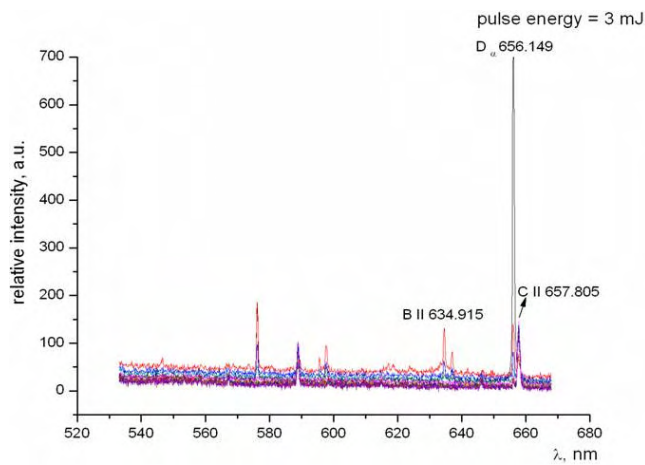


Figure 3.2.6.1, b: The spectra after 9 consecutive pulses.

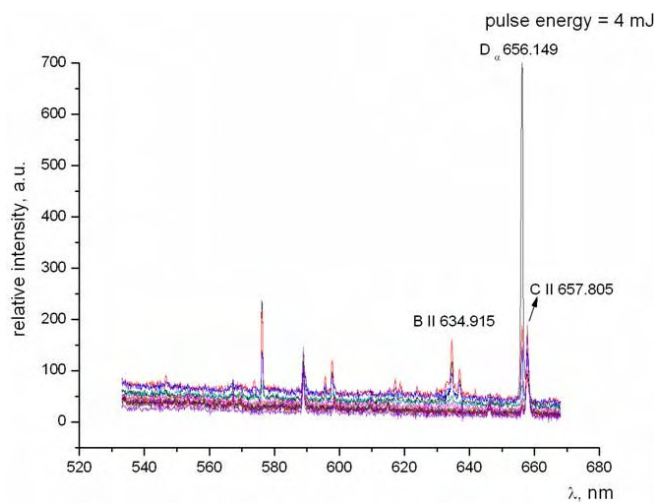


Figure 3.2.6.1, c: The spectra after 9 consecutive pulses.

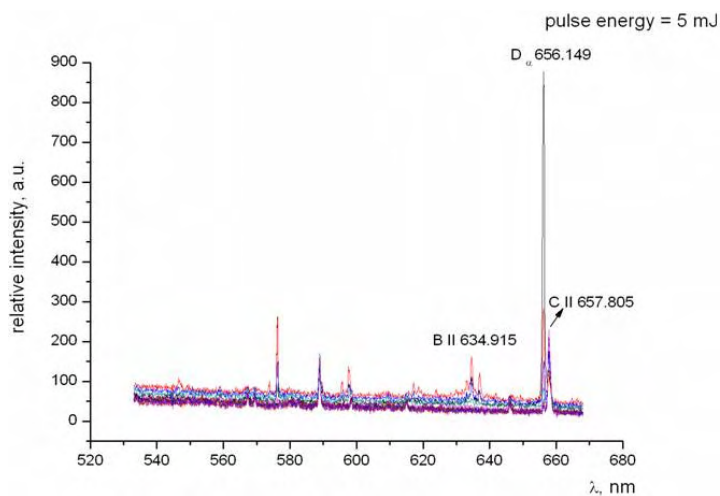


Figure 3.2.61, d:
The spectra after 9 consecutive pulses.

Concerning depth profiles of the impurities, the corresponding curves are represented in Fig. 6.2.

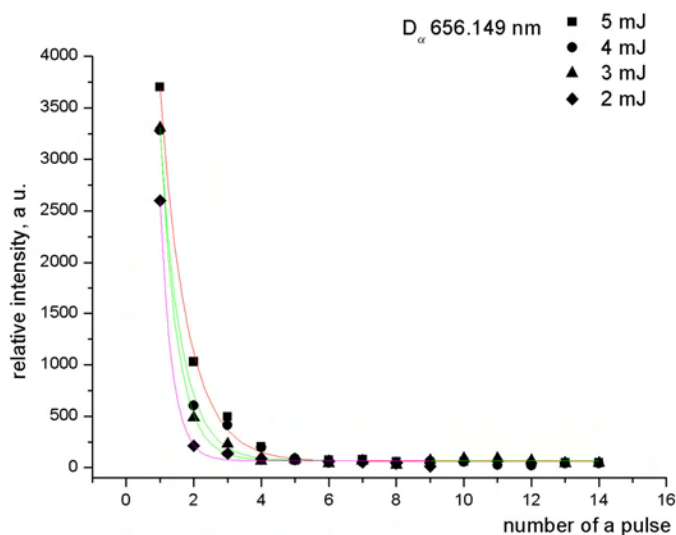


Figure 3.2.6.2. Depth profiles of D_{α} line ($\lambda=656.15$ nm) at different energies of laser pulses. The index number of a pulse in the sequence is shown on the X axis. The estimated thickness of the ablated layer according to the crater depth profile is $\Delta=190$ - 220 nm

Appearing after the 1st laser pulse and showing the maximal intensity, the sharp decrease of the deuterium signal with growing of the number of applied pulses is observed. After applying the 2nd laser pulse the intensity of D_{α} line has decreased almost six times compared to that after the 1st pulse. The signal of deuterium line becomes almost equal to the background level after applying the 4th laser pulse.

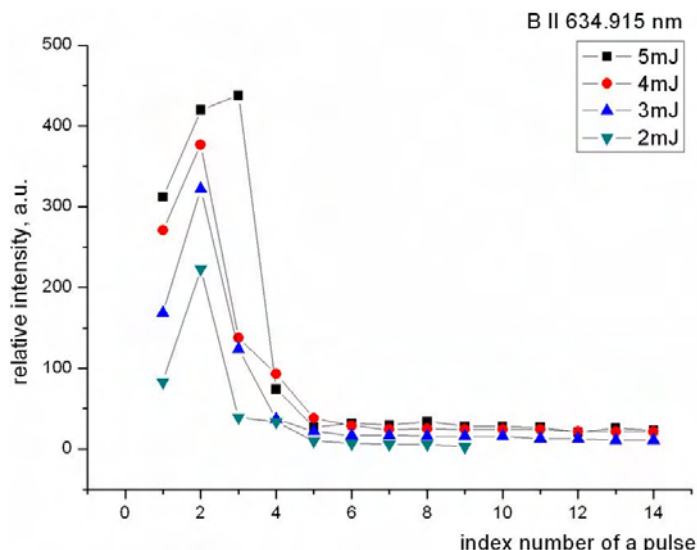


Figure 3.2.6.3. Depth profiles of BII line (634.91 nm) at different energies of laser pulses. The index number of a pulse in the sequence is shown on the X axis

The evaluation of the intensity of BII 613.91 nm line differs from that of deuterium. In contrast, the maximum has been reached after the second laser pulse, but for the ablation at 5 mJ – the third pulse – was applied to the target. With the fourth pulse, the intensity of the BII line has decreased 5 times in comparison to the second pulse, and after the fifth pulse is almost equal to the background level.

As for CII 657.8 nm line, the intensity dependence on the number of laser pulses applied to the target is completely different.

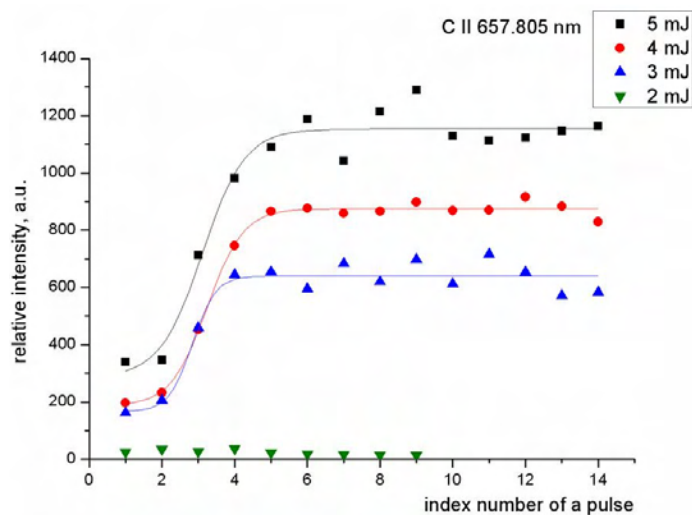


Figure 3.2.6.4. Evolution of CII line ($\lambda=657.8$ nm) with the number of applied pulse at different pulse energy. The index number of a pulse in the sequence is shown on the X axis

As graphite is the basic material of ASDEX Upgrade samples, the intensity of the CII 657.8 nm line is growing with the number of the applied pulses, and after the 5th pulse the signal remains approximately constant. The intensities corresponding to the ablation at pulse energy 2 mJ are nearly constant and equal to the background level as ablation threshold of the graphite is exceeded very little.

The Figs. 3.2.6.1-6.4 demonstrates the spectra obtained after ablation of the AUG tile sample #2.1. The concentration of deuterium measured with RBS is 5.84×10^{17} atoms/cm³, the concentration of boron – 1.11×10^{19} atoms/cm³. Considering the ablation removal rate in the case of applying 2-5 mJ, the results show that the almost all the deuterium found in AUG sample is released from the depth of 0.5-1 μm inside the material. The concentration of boron is maximal at ~1μm depth, then the concentration decreases.

▪ **Carbon tile #2.2**

For investigation of the evaluation kinetics of the laser induced plasma, the emission spectra have been measured in 5 ns time gate at different delay time intervals after the laser pulse. The CII line has been the choice instead of the deuterium line because the latter decays strongly with the number of applied laser pulses.

The results are represented in Figs 3.2.6.5-6.7.

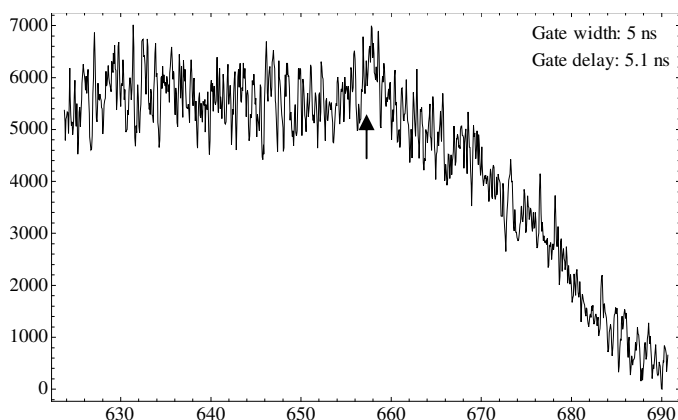


Figure 3.2.6.5. The laser induced plasma emission spectrum during time gate 5 ns delayed for 5.1 ns with respect to the 0.18 ns laser pulse (1024 nm, 5 mJ)

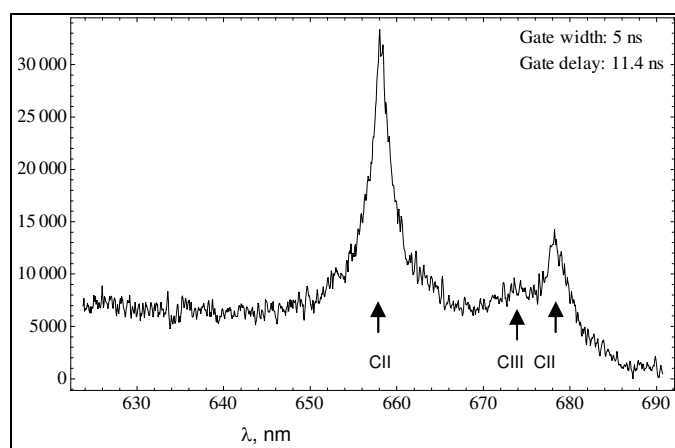


Figure 3.2.6.6. The laser induced plasma emission spectrum during time gate 5 ns delayed for 11.5 ns with respect to the 0.18 ns laser pulse (1024 nm, 5 mJ)

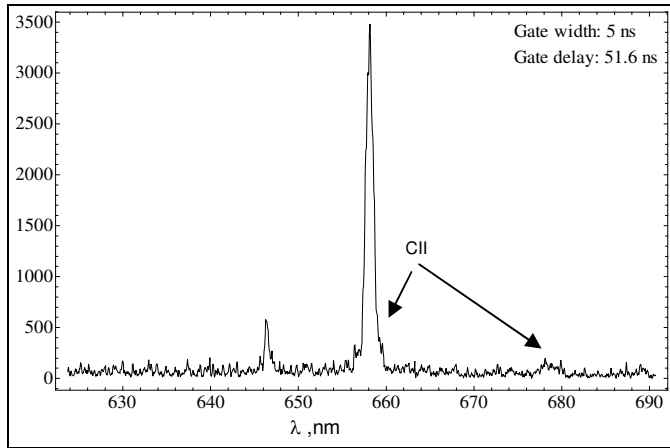


Figure 3.2.6.7 The laser induced plasma emission spectrum during time gate 5 ns delayed for 51.1 ns with respect to the 0.18 ns laser pulse (1024 nm, 5 mJ).

During the first few nanoseconds after the picosecond pulse only thermal emission of ablated plasma occurs (Fig. 3.2.6.5). The broadened CII line exceeding the intensity of the thermal emission about five times is present (Fig. 3.2.6.6.). The background of the thermal emission considerably decreases in tens of nanoseconds, and only slightly broadened line emission of the main CII line in the observed spectral region is present (Fig.3.2.6.7). Thus, for measurements of the full light-sum, it is preferable to perform measurements with delay starting from approximately 15 ns.

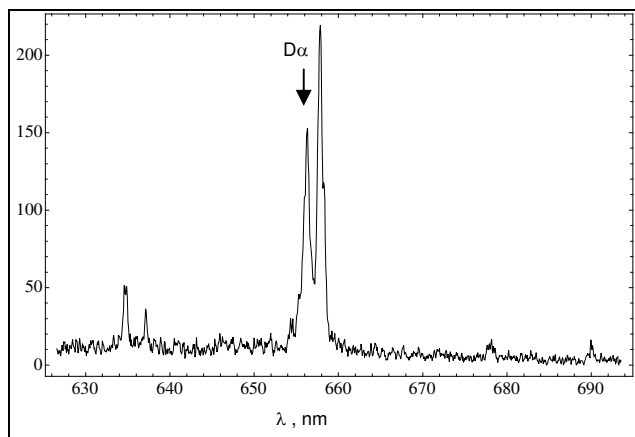


Figure 3.2.6.8. The laser induced plasma emission spectrum during the first shot

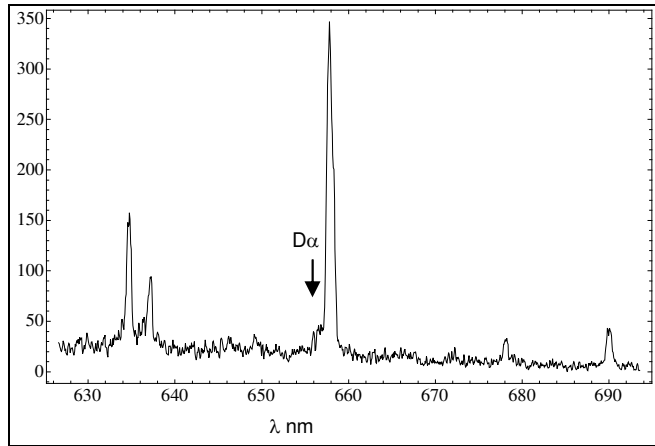


Figure 3.2.6.9. The laser induced plasma emission spectrum during the second shot

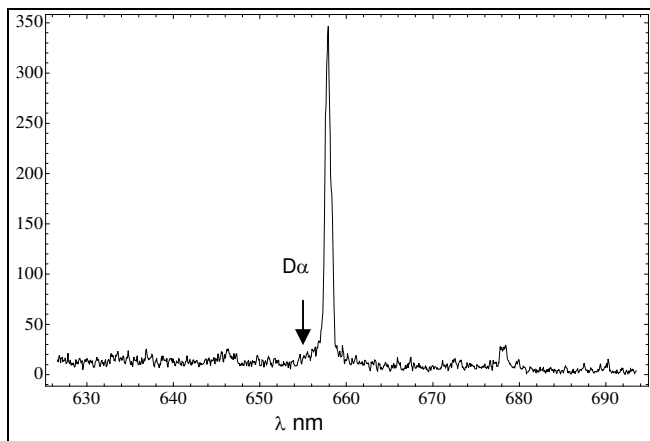


Figure 3.2.6.10. The laser induced plasma emission spectrum during the second shot

Using delayed laser induced plasma emission measurements the evaluation of the concentration in consecutive single laser pulse sequence has been performed. Already during the second shot the D_{α} intensity decreases about of eight times. The corresponding D_{α} depth profile is represented in Fig. 3.2.6.14.

- **W-coated tile #3**

The laser induced plasma spectra in consecutive single laser pulse sequence for W-coated sample of tile #3 is represented in Figs. 3.2.6.11-6.13.

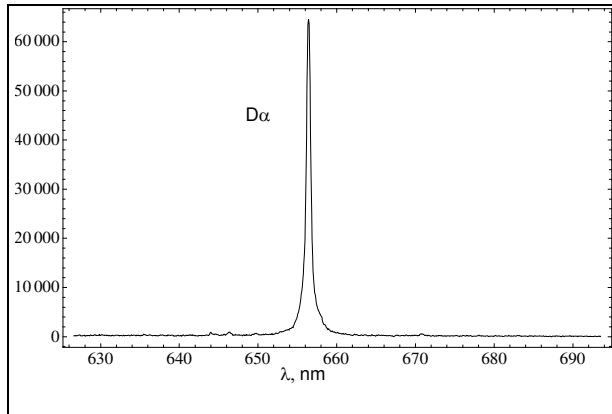


Figure 3.2.6.11. The laser induced plasma emission spectrum during the first shot.

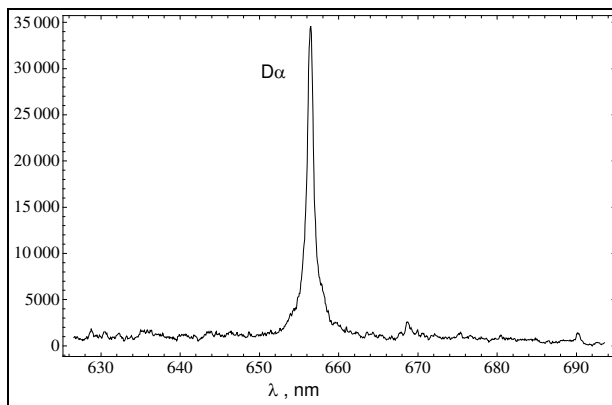


Figure 3.2.6.12. The laser induced plasma emission spectrum during the second shot.

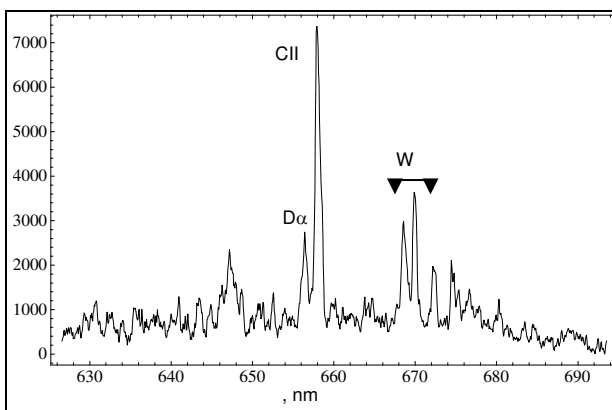


Figure 3.2.6.13. The laser induced plasma emission spectrum during the sixth shot.

The composition of chemical elements in the W-coated tile is quite different compared to the carbon-based tiles. The upper layer mainly consists of some deuterium related compounds not discovered in the present experiments (Fig. 3.2.6.11). Already in the second shot the intensity of the D_{α} line is decreased twofold, and trace lines of tungsten appeared (Fig. 3.2.6.12). Fig. 3.2.6.13 shows that three

elements are simultaneously present in the corresponding layer – deuterium, carbon and tungsten.

Fig. 3.2.6.14 summarizes the depth profiles of deuterium in carbon based and W-coated carbon tiles of AUG as well as the characteristic depth profile of deuterium, carbon and tungsten in the sample of W-coated tile.

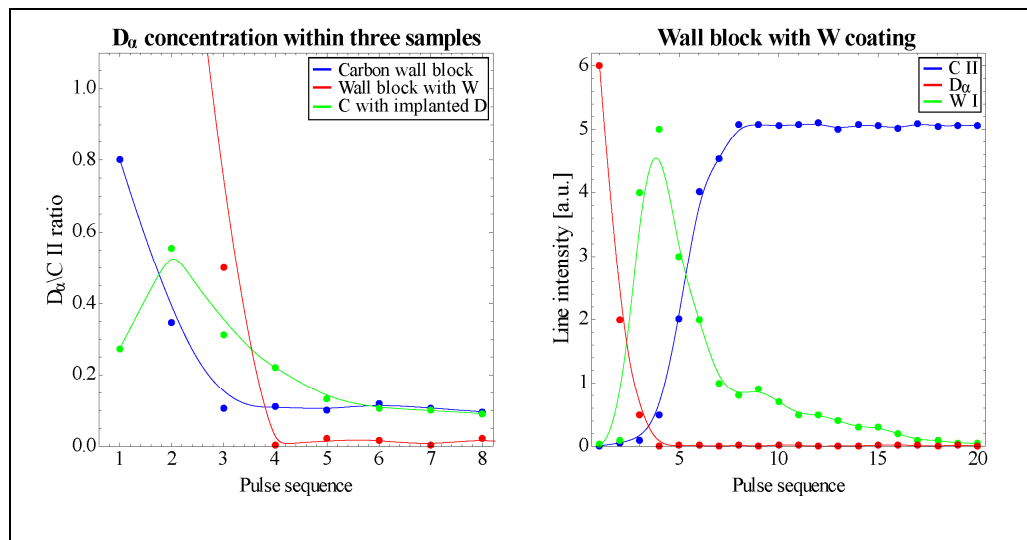


Figure 3.2.6.14. Left graph: The concentration ratio D_{α}/CII removed by the sequence of single laser pulses: green line – the implanted carbon 6710 reference tile #1, blue line – the post mortem graphite tile #2.2, red line – post mortem W-coated graphite tile #3.

Right graph: The emission line intensity dependences on the sequence of single laser pulses in the post mortem W-coated graphite tile: red line – D_{α} ; green line – W; blue line – C II.

In the post mortem tiles, the concentration of deuterium decreases during the first few laser pulses and corresponds to the layer depth of 0.8 to 1.2 μm . In implanted reference sample, the maximum concentration of deuterium is about 200 μm .

In post mortem W-coated sample, deuterium is accumulated mainly above the tungsten layer. The results of SEM analysis show that deuterium is partially dissolved in the tungsten layer. The growth of carbon content in the region of tungsten layer according to the SEM data indicates that a single ablation event can build destroyed islands in the tungsten layer leading to appearance of the carbon line in the spectrum. In the bulk graphite, the concentration of tungsten slowly decreases. The penetration depth of tungsten reaches 4 μm .

7. Solutions and resources for *in situ* out-of-vessel LIBS spectroscopy

For *in situ* implementation of LIBS spectroscopy, only one common optical port will be available to access the wall. We assume that the diameter of the optical window will be at least 100 mm.

Distance from the optical port to the opposite wall of vessel can reach from about 4 m to about 10 m.

The implementation of LIBS spectroscopy can be reduced to the two main problems:

- a) Methods to focus and position the laser beam(s) on the surface of the wall;
- b) Methods to enhance both the efficiency of plasma emission by the laser heating technique and to eliminate the plasma thermal emission background from the spectral line emission of plasma atoms and ions.

7.1. Optical lens system for laser beam focusing

To focus the laser beam, the objective available for the visible spectral region has been set up. Taking into account that the optical characteristics – transmittance and focus – strongly depends on the wavelength the focusing experiments have been performed using the second harmonic of Nd:YAG laser (SL312).

The simplest mechanical assembly of the objective elements have been used to vary its focal length, consisting from two positive (convex) lenses a negative (concave) lens between them. Moving the concave lens, the focal length will be changed.

Using high basis length of objective (distance between light the input and output lenses) the focal length of the objective can be adjusted with high accuracy.

Modelling the optical power of the lenses (in dioptries) the following objective lenses have been set up (Fig. 3.2.7.1):

- 1) Positive (convex) lens at a distance = 0 cm (fixed); focus = 800 mm, 1.25D;
- 2) Negative (concave) lens at a distance = from 50 mm to 250 mm (variable); focus = 680 mm, 1.45D;
- 3) Positive (convex) lens - distance = 310 mm (fixed); focus = 4000 mm, 0.25

D.

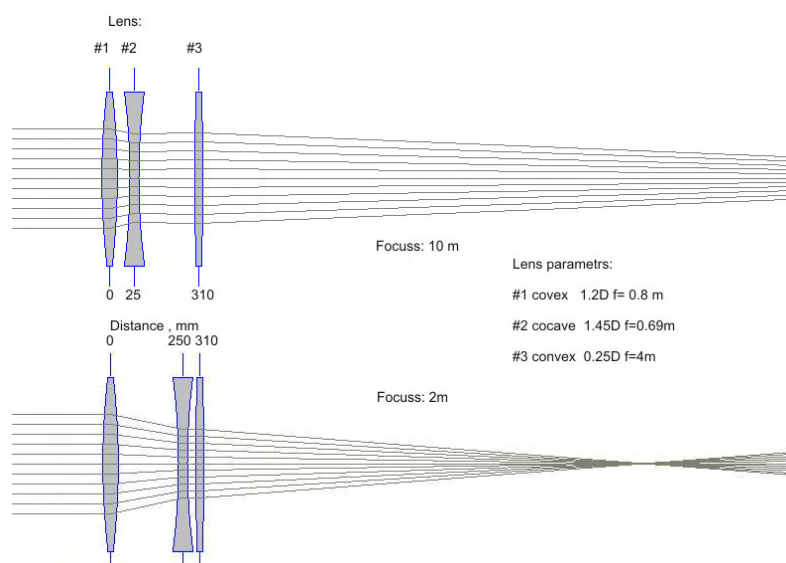


Figure 3.2.7.1. The sketch of the objective for focusing the laser beam

The concave lens has been moved using XY translation stage. The objective has been successful tested for objective – target distance from 3.5m to 10m.

7.2.Sensitivity of the spectroscopy system for *in situ* measurements

The maximum aperture is defined by the diameter of the port and a distance to the target.

For modelling the light collection characteristics the objective lens of the experimental laboratory setup has maximal aperture $f/4$ corresponding to the aperture of the used spectrograph. Using adjustable diaphragm in front of objective lens, the measurements at the aperture values for different distances from optical port (diameter = 100 mm) were performed. The emission was focused on the fibre bundle and transferred to the entry slit of spectrograph. The gain of ICCD camera was set to 90 to prevent the overload of the ADC converter of the ICCD camera. The maximal gain of the camera is 200, thus allowing to increase the sensitivity of the spectra measurements more than twofold.

Fig. 3.2.7.2 represents the results.

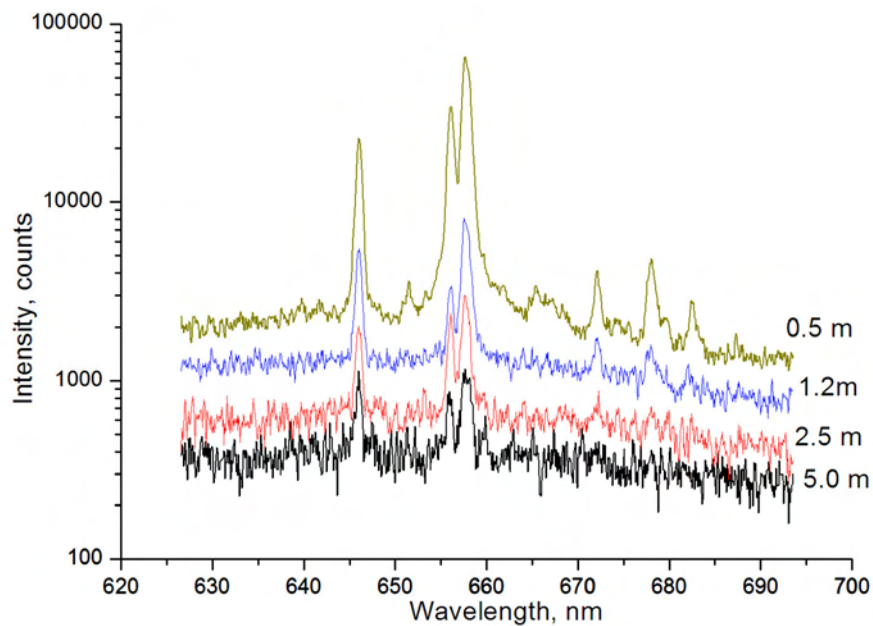


Fig.3.2.7.2. The D_{α} and CII emission lines obtained for post mortem graphite tile #2.2 sample during the first laser shot at different apertures

Results show that using a full gain of the ICCD camera, the present spectral setup provides the measurements of the tungsten and carbon II lines at intensities covering two orders of magnitude. They correspond to the distance optical port - target from 0.5 m to 5.0 m.

Extension of the application of LIBS spectroscopy to the larger distance optical port – target needs to enhance the efficiency of plasma emission by the laser heating technique.

The alternative is increasing the ablation pulse energy and, as a result, simultaneous increasing of the crater diameter.

7.3. The laser heating technique

The preliminary experiments were performed by ablating the Al targets. The results show that the plasma heating efficiency sufficiently increases using short wavelength laser pulses instead of 1064 nm Nd:YAG emission.

For the laser heating experiments, two beams of the SL312 laser was applied. The 1064 nm pulse was used to form the plasma plume, and the fourth harmonic 253 nm pulse to perform the plasma heating. Both pulses have been focused on the target. The delay between 1064nm and 253nm pulses was adjusted by the distance of the 253nm beam between the laser head and target.

The results of the plasma heating effect are shown in Fig. 3.2.7.3.

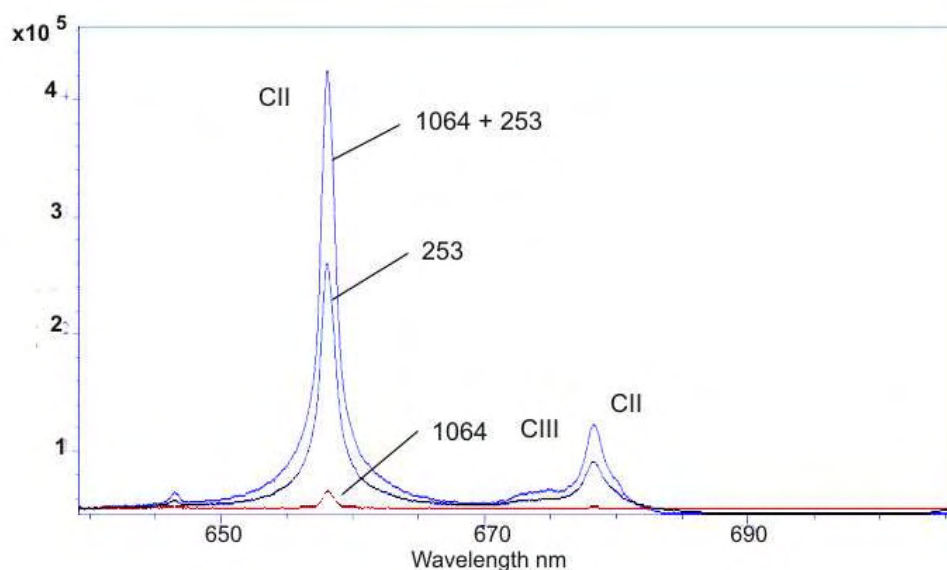


Figure 3.2.7.3. The CII line intensities excited by 1064 nm 4mJ pulse, excited by 253 nm 180mJ pulse, excited by 1064nm 4mJ pulse and heated by 253nm 18mJ pulse delayed for 12 ns.

The light-sum of the CII line excited by 4mJ 1064nm pulse (0.12×10^{-9} s) after applying 180mJ 253nm pulse increases for about 30 times. The ablation light-sum for single 253 mJ pulse exceeds the light sum of the 4mJ 1064nm pulse for about 20 times. In absence of the early excited plasma plume the focused 253 mJ pulse results in ablation of the target material.

Results of the time-resolved spectroscopy show the plasma evaluation after excitation and heating (Figure 3.2.7.4).

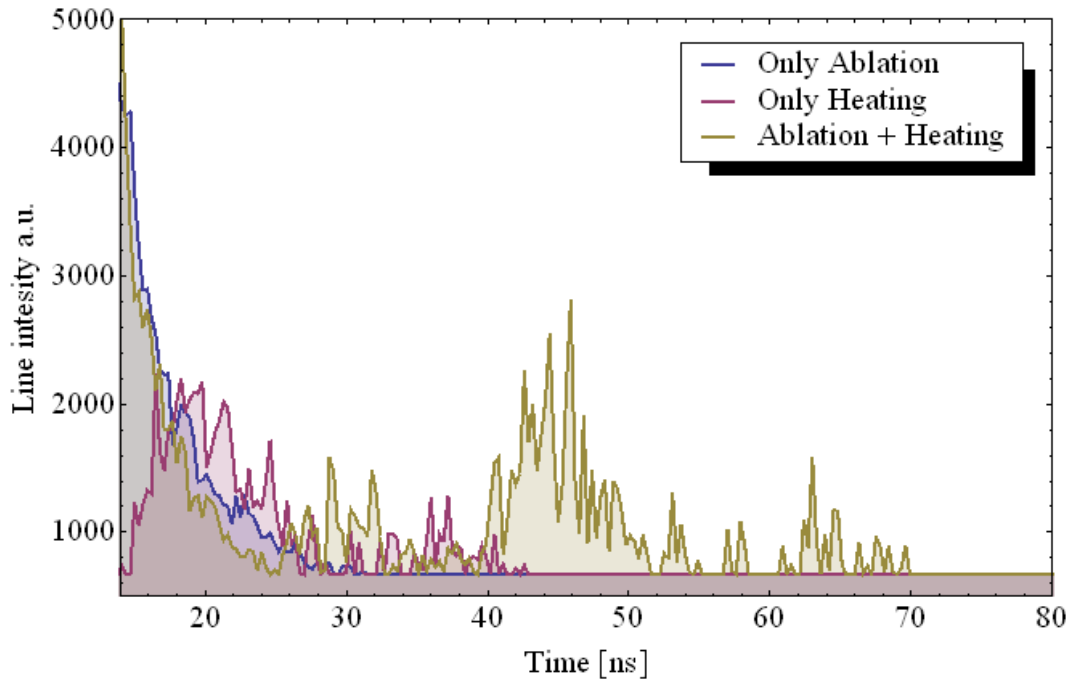


Figure 3.2.7.4. The decay kinetics of the CII line after applying the 0.12ns heating laser pulse (14ns delay with respect to the 1064ns pulse).

The blue curve shows that the decay of the CII line intensity after exciting with the 4mJ 1064nm pulse is followed by the exponential decay within about 30 ns. The decay of the CII line after heating with 2553nm 0.12ns pulse shows that the heating pulse leads to decrease of the intensity compared to that without heating. The main effect of the heating pulse is long-time CII line afterglow up to about 70 ns. Afterglow results in the considerable enhance of the light-sum emitted due to the plasma excitation with the second laser pulse.

The long-lived relaxation occurs in cold plasma and is caused by the relaxation in highly excited electron states of plasma atoms and ions.

The decrease of the CII line intensity after the heating laser pulse in the early stages of decay indicates that the 254nm photons are effectively absorbed by the carbon atoms an ions and transformed to the high excited state.

8. Conclusions

- The setup for development the advanced LIBS spectroscopy of impurity distribution has been constructed. The following equipment and techniques have been implemented: the double-pulse laser beam system for ablation plasma heating; the laser pulse energy measurements; the ICCD camera purchased and single photon sensitivity time resolved spectroscopy developed. The equipment for the experimental testing of the LIBS spectroscopy for feasibility of *in situ* impurity analysis has been developed and characteristics of the laser beam focusing, measurements at different wall – optical port distances, plasma heating were investigated. The laser beam pulse energy and profile settings have been optimized by investigation the crater shape and surface structure formation using the profiler and the SEM. Plasma plume

spectroscopy and deuterium, boron and carbon line distribution have been investigated in three types of ASDEX tile samples: D-implanted, post-mortem and W-coated graphite.

- The scientific results. Formation of the flat ablation crater occurs when the laser pulse energy density reaches values above 10^{10} W/cm², corresponding to the direct ionization of target material. The ablation results in formation of isolated dust particles on the crater surface. The efficiency of the plasma heating increases by use of the high photon energy laser pulses. Using sub-nanosecond laser pulses (0.18 ns), cold ablation plasma occurs after 10-15 ns. Further, the thermal background emission is eliminated.
Feasibility of *in situ* LIBS spectroscopy. The objective having a high basis length satisfied the focusing of the laser beam up to 10 m. The laser heating technique results in increase of the light sum emitted by atoms for at least two orders of magnitude being additionally excited to the high energy states.
The use of the ICCD camera in the time-resolved regime provides measurements of the spectral lines with accuracy of 5% at the intensities covering two orders of intensity (0.5-5m for the diameter of the optical window of 100 mm). Application of the plasma heating extends the available emission acquisition distance up to 10 m.

3.3. Theory and code development

Principal investigator: **Dr. V. Kuzovkov**

O. Dumbrajs, G. Zvejnieks, E. Kotomin, Yu. Zhukovskii, A. Gopejenko

3.3.1. Stochastization of magnetic fields and magnetic reconnection

The role of stochastization in fast MHD phenomena in ASDEX Upgrade

O. Dumbrajs¹, V. Igochine², A. Gude², K. Lackner², M. Maraschek², G. Pereverzev², H. Zohm², and ASDEX Upgrade team²

¹Association Euratom/University of Latvia, Latvia

²Association Euratom/IPP Garching, Germany

Studies of fast MHG events in ASDEX Upgrade suggest that stochastization plays an important role in these processes. In spite of the short time duration and the small region, stochastization can lead to significant changes in plasma confinement. The main reason for this is a strong mixing of the magnetic field lines which destroys magnetic surfaces and strongly increases the radial transport. In the present talk two such phenomena will be discussed: the frequently interrupted regime of neoclassical tearing modes [1,2] and the sawtooth crash [3]. The role of stochastization of magnetic field lines is analyzed by applying the mapping technique to trace the field lines of toroidally confined plasma [4]. The proposed stochastic model for the sawtooth crash is able to explain fast losses of heat from the plasma core with simultaneously small changes of the safety factor profile [5]. Here the sawtooth crash does not change the position of the $q=1$ surface. This observation disagrees with ordinary sawtooth models, but is in agreement with the stochastic picture of the crash. The sawtooth crash dynamics is also studied by means of the spectral analysis and reconstruction of phase trajectories using the delay coordinates to identify the road to chaos in different physical systems [6].

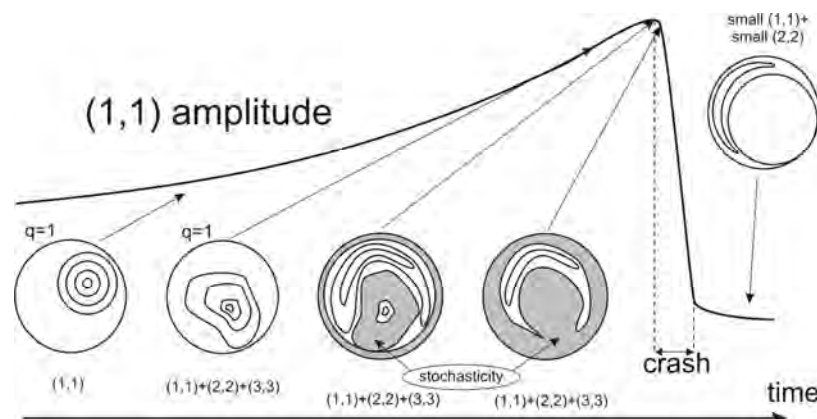


Figure 3.3.1.1. The temporal evolution of a sawtooth crash. Close to the crash phase higher harmonics grow and deform the surface, but only after reconnection stochastization becomes possible which leads to the crash.

References

1. O. Dumbrajs, V. Igochine, D. Constantinescu, H. Zohm, and ASDEX Upgrade team, Phys. Plasmas **12** (2005) 110704.

- .2. V. Igochine, O. Dumbrajs, D. Constantinescu, H. Zohm, and G. Zvejnieks, Nuclear Fusion **46** (2006) 741.
3. V. Igochine, O. Dumbrajs, H. Zohm, and A. Flaws, Nuclear Fusion **47** (2007) 23.
4. D. Constantinescu, O. Dumbrajs, V. Igochine, and B. Weyssow, Nucl. Fusion **48** (2008) 024017.
5. O. Dumbrajs, V. Igochine, and H. Zohm, Nucl. Fusion **48** (2008) 024011.
6. V. Igochine, O. Dumbrajs, and H. Zohm, Nucl. Fusion **48** (2008) 062001.

Temporal evolution of neoclassical tearing modes in the frequently interrupted regime

O. Dumbrajs¹, V. Igochine², A. Gude², M. Maraschek², H. Zohm² and ASDEX Upgrade Team²

¹*Institute of Solid State Physics, Association Euratom-University of Latvia,
Kengaraga Street 8, LV-1063, Riga, Latvia*

²*MPI für Plasmaphysik, Euratom-Association, D-85748 Garching, Germany*

Abstract

A phenomenological method for description of temporal evolution of neoclassical tearing modes in the frequently interrupted regime (FIR) is proposed. The method makes it possible to predict the beginning and the end of the FIR regime as well as the frequency of the FIR drops. A few experimental parameters which are used in the model are commonly measured quantities. Several specific ASDEX Upgrade ([http://en.wikipedia.org/wiki/ASDEX Upgrade](http://en.wikipedia.org/wiki/ASDEX_Upgrade)) FIR discharges with different heating and different FIR behaviour are analyzed in detail.

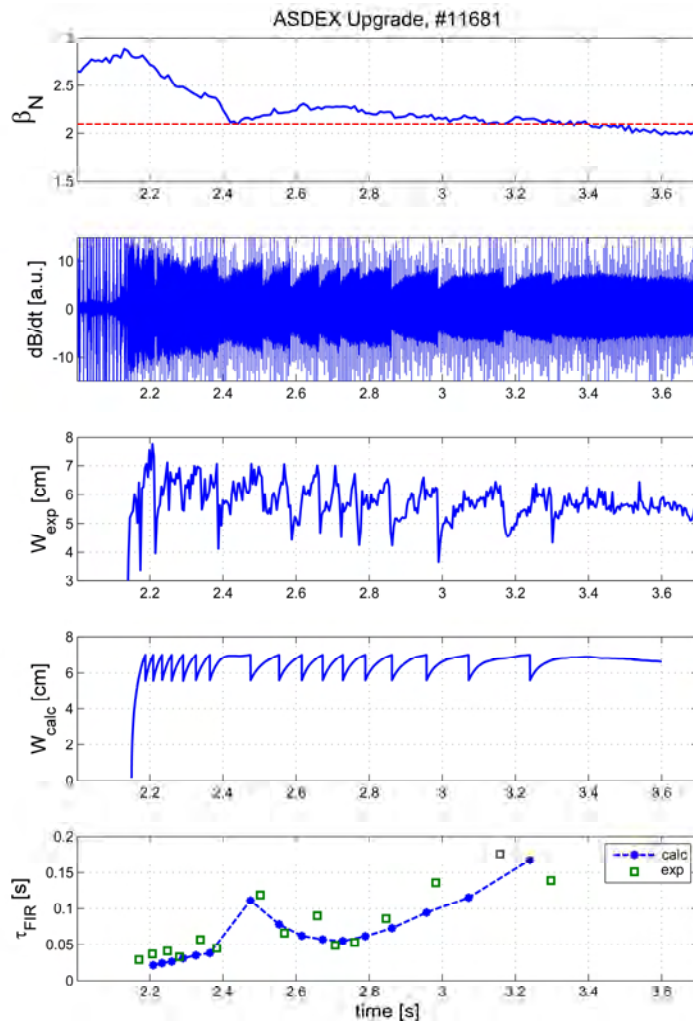


Figure 3.3.1.2. (Color online) Temporal evolution of β_N , dB/dt , W_{exp} , W_{calc} , and τ_{FIR} . The red dashed line marks the border line between absence (below) and presence (above) of FIR phenomenon. The heating power was reduced by 2.5 MW between 2.38s and 2.42s which causes the fast β_N drop during this time. Here $\alpha = 85500$.

3.3.2. Radiation stability of reactor materials

1. Objectives

The experimental studies of novel materials for fabrication of radiation resistant materials for nuclear reactors (technical task TW3-TPDC-IRR CER Euroatom-Latvia performed in 2004 and lead by Prof. A. Sternberg) suggested to study oxide-dispersion strengthened steels (ODS) as reduced activation ferritic-martensitic structural materials for prospective fusion reactors. Reduced activation steels strengthened by yttria precipitates are considered as promising structural materials for future fusion- and advanced fission-reactors. In particular, application of oxide dispersion strengthened (ODS) steels for fusion reactor blanket structure allows increasing its operation temperature by $\sim 100^\circ\text{C}$. Both size and spatial distributions of

oxide precipitates significantly affect mechanical properties and radiation resistance of ODS steels. However, the mechanism of ODS nanoparticle formation is still not well understood. The aim of our theoretical study in 2009 has been to continue the first principles modeling of ODS steels accompanied by kinetic Monte-Carlo simulations, in order to clarify a growth mechanism of ODS nanoparticles and conditions of their stability inside the *fcc* iron lattice.

2. Introduction

Some recent experiments indicate that at least part of yttrium oxide particles might be dissolved in the steel matrix during mechanical alloying [1-3]. If so, yttrium dissolved above its equilibrium solubility limit will precipitate during hot isostatic pressing of mechanically alloyed powder. Slow diffusion of large substitutional yttrium atoms is probably a limiting factor for yttrium oxide particle growth. Diffusion of interstitial oxygen is much faster and, therefore, cannot delay the growth w Y-vacancy pair as a simplest diffusing yttrium-containing complex. In our model iron matrix is represented by a face-centered cubic γ -Fe lattice, which is stable at typical hot isostatic pressing temperatures. We have performed the first principles DFT calculations of different pair and triple point defect complexes containing: (i) the two yttrium atoms substituted for iron lattice atoms, (ii) the Y-Fe-vacancy pairs and (iii) the oxygen impurity atoms dissolved in the steel matrix. The latter is modeled as a face-centered cubic γ -Fe single crystal, while transition to γ -phase occurs in low Cr ferritic-martensitic steels at typical hot isostatic pressing temperatures.

3. Results

VASP-4.6 computer code with a plane-wave basis set [4] has been used for large-scale first-principles parallel calculations on both perfect and defective *fcc* lattice of γ -Fe phase. Perdew-Wang-91 GGA (Generalized Gradient Approximation) non-local exchange-correlation functional and the scalar relativistic PAW (Projector-Augmented Wave) pseudopotentials are used for these calculations performed in parallel regime with a total geometry optimization. The pseudopotentials describe the core electrons of Fe ($4s^1 3d^7$ outer shell), O ($2s^2 2p^4$) and Y ($4s^2 4p^6 5s^1 4d^2$) atoms with 8, 6 and 11 external electrons, respectively. Preliminary test calculations show that the results are converged only for the large supercells (containing more than 64 atoms) and cut-off energies of 800 eV), which requires exceptional computational resources. Varying the k-point set, it has been found that at least $12 \times 12 \times 12$ mesh allows us to obtain more-or-less plausible results for $4 \times 4 \times 4$ supercell and for larger supecells it is necessary to use the largest *k*-point mesh possible that does not exceed the memory limits.

After completing the calculations of the configurations with single point defects, we have proceeded with the modeling of the defect pairs. The charge redistribution plots were constructed for all corresponding models. The calculations of the interaction between the Y substitute and Fe-vacancy at different inter-distances have been performed first (Fig. 3.3.1.1). The formation and binding energies of the pair of yttrium atoms were calculated. The modeling showed that attraction is found for the 1-NN, 3-NN and 4-NN configurations while the repulsion is observed for the 2-NN configuration. The relative displacement of Y atom in the 1-NN configurations is the most significant (1.25 Å) and the binding energy is the largest (1.67 eV).

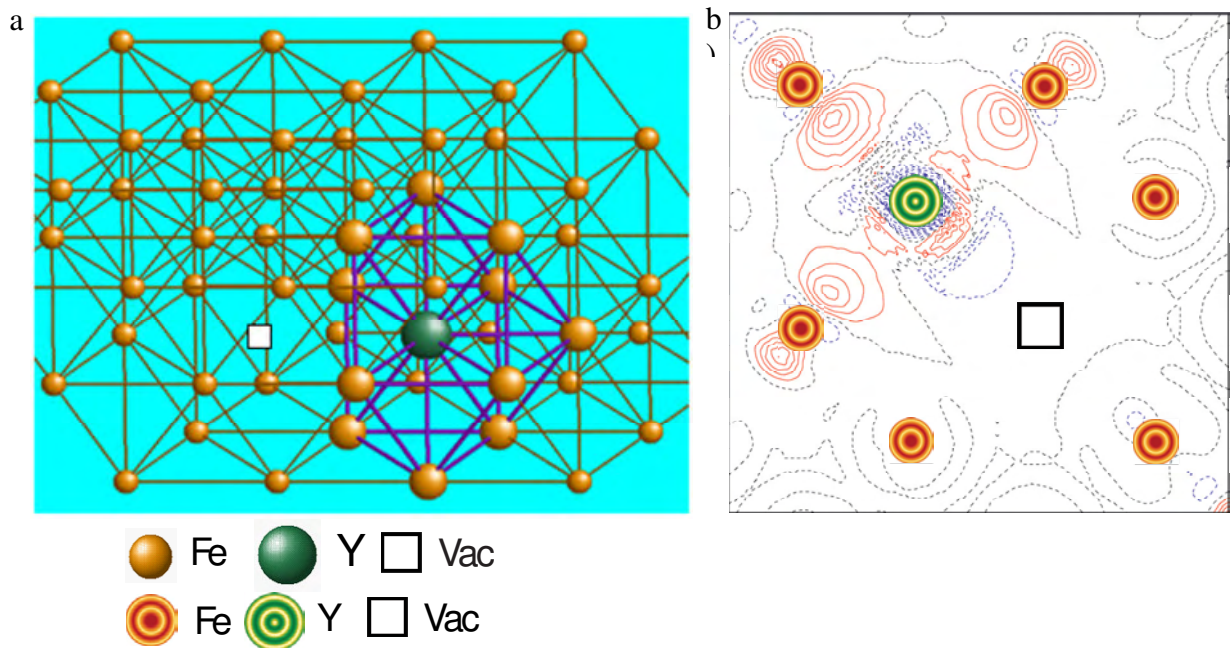


Figure 3.3.2.1. The model of Y substitute atom and Fe-vacancy in 1NN positions (a) and the corresponding electron charge redistribution (b) in *fcc* Fe lattice

The results presented in Table 1 confirm aforementioned expectations. Relative displacement of Y atom in the 1-NN configurations is the most significant (1.25 Å) and the binding energy is the largest (1.67 eV). In the 2-NN configuration there is no bonding between the Y substitute and Fe vacancy and in the 3-NN and 4-NN configurations of this pair the binding energies are 0.30 eV and 0.40 eV, respectively.

At the next step, the interaction of two yttrium substitutional atoms at different interdistances has been calculated. The model of two Y substitute atoms in *fcc* Fe lattice at the first nearest neighbors (NN) positions is shown in Fig. 3.3.2.2a and the corresponding electron charge redistribution is presented in Fig. 3.3.2.2b.

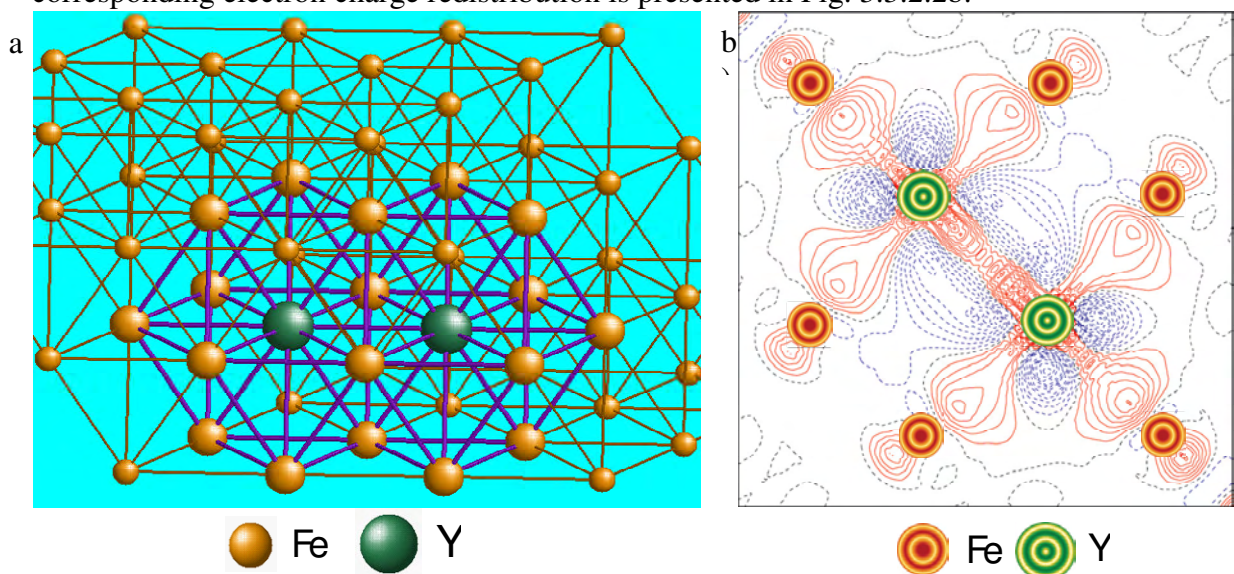


Figure 3.3.2.2. The model of two Y substitute atoms in 1NN positions (a) and the corresponding electron charge redistribution (b) in *fcc* Fe lattice

The analysis of the calculations showed that no bonding was found between the two yttrium atoms in the iron lattice at any distance. Some enhancement of the electron density between Y-Y pair can be visible as compared to the configuration of yttrium atom and iron vacancy (Fig. 3.3.2.2), *i.e.*, the repulsion between the two Y substitutes is smaller than that between Y and Fe atoms.

As no bonding was found between 2 Yttrium substitutes (1-NN neighbors) we supposed that addition of oxygen atom in the *O* site would construct the more stable solute atom configuration and have calculated three-atom configuration (Fig. 3a) and the corresponding charge redistribution around the 2 Y substitutes and O atom.

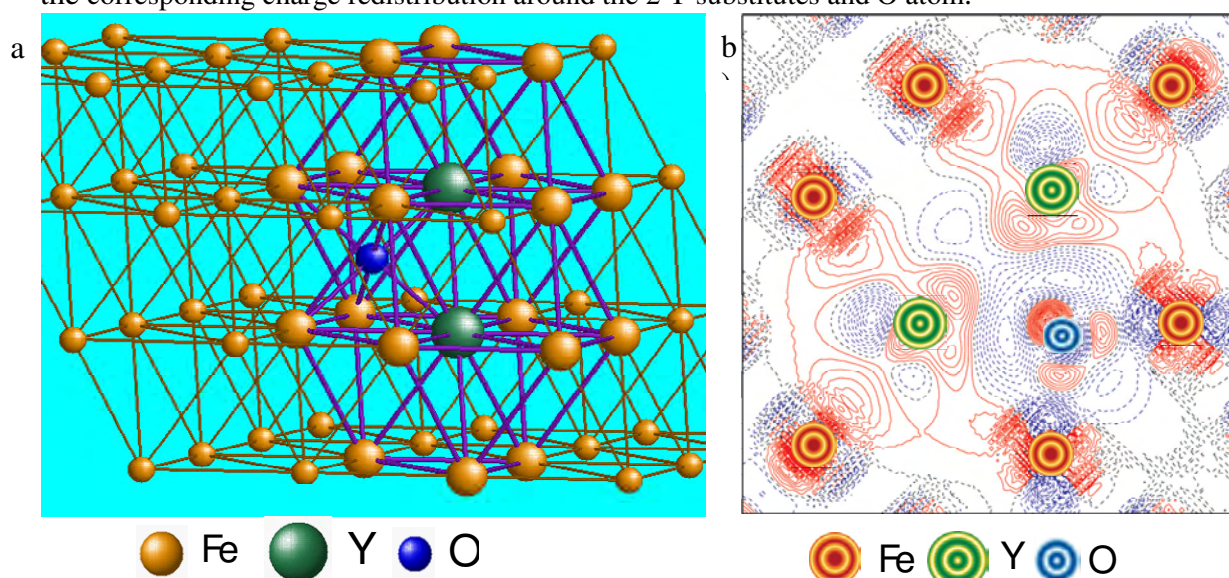


Figure 3.3.2.3. The model of the γ -Fe crystalline lattice with 2 Y substitutes and 1 O impurity atom in the 1st nearest neighbors positions (a) and the corresponding charge redistribution around the 2 Y substitutes and O atom.

No bonding has been found in this nanocluster inside the γ -Fe lattice as compared to equilibrium of Y_2O molecule. Significant displacements were observed during relaxation between each pair of Y and O atoms, achieving 0.45 Å for yttrium, whereas Y atoms move from each other by 0.37 Å. Resulting Y_2O configuration inside the γ -Fe lattice does not correspond to the equilibrium Y-O-Y structure of the nearest oxygen and yttrium atoms in any Y_2O_3 crystalline phase. These results allow us to propose that only the increased concentration of Fe vacancies can really assist to the formation of the Y_2O_3 precipitates inside the γ -Fe lattice.

4. Summary

Our calculations clearly show that no bonding occur between 2 Y atoms at different mutual distances. The addition of O atom in the interstitial octahedral position as the 1NN increases the repelling force between 2 Y atoms which leads to complete loss of interaction between 2 Y atoms. We assume that interaction between atoms in 2 Y atom and O atom complex should occur when atoms are placed at 2NN positions. The presence of vacancy could also positively affect the interactions between atoms in this complex.

To simulate the yttrium migration inside *fcc* Fe lattice the configurations of Y-Fe vacancy pairs at different mutual distances have been used. The preliminary analysis of these calculations showed the insufficient mobility of impurity atom and single vacancy complex. To increase the mobility of yttrium atom inside iron lattice, we should consider a presence of more than one neighbouring Fe vacancy. Thus, the next

step in our research is to perform the large-scale calculations of yttrium in *fcc* iron lattice with 2-3 or even more vacancies.

References

1. R. Lindau, A. Möslang, M. Rieth, M. Klimiankou, E. Materna-Morris, A. Alamo, A.-A. F. Tavassoli, C. Cayron, A.-M. Lancha, P. Fernandez, N. Baluc, R. Schäublin, E. Diegele, G. Filacchioni, J.W. Rensman, B.v.d. Schaaf, E. Lucon, and W. Dietz, *Fus. Eng. Design* 75–79, 989 (2005).
2. M. Klimiankou, R. Lindau, A. Möslang, *J. Nucl. Mater.* 367–370, 173 (2007).
3. M. Klimenkov, R. Lindau, A. Möslang, *J. Nucl. Mater.* 386–388, 553 (2009).
4. G. Kresse and J. Haffner, *VASP the Guide*. University of Vienna, Austria, (2009).

Collaborations

1. Karlsruhe Institute of Technology, IMF-1, Germany
2. RRC Kurchatov Institute, Kurchatov Sq. 1, 123182 Moscow, Russian Federation

Presentations at conferences in 2009

1. A. Gopejenko, Yu.F. Zhukovskii, P.V. Vladimirov, E.A. Kotomin, and A. Möslang, "Simulation of yttrium and oxygen solute atoms in *fcc* Fe lattice in support of ODS steel development. 25th ISSP scientific conference (Riga, Latvia, February, 2009). Abstracts: p. 55.
2. A. Gopejenko, Yu.F. Zhukovskii, P. Vladimirov, E.A. Kotomin, and A. Moslang, "Simulations on solution of yttrium and oxygen atoms in *fcc* iron lattice". International conference "Functional materials and nanotechnologies" FM&NT-2009 (Riga, Latvia, April, 2009), Abstracts: p. 101.
3. A. Gopejenko, Yu.F. Zhukovskii, P.V. Vladimirov, E.A. Kotomin, and A. Möslang, "Simulation of yttrium oxide particle formation in iron in support of ODS steel development". 6th International Conference "Information Technologies and Management", IT&M'2009 (Riga, Latvia, April, 2009). Abstracts: pp. 30-31.

4. EFDA FUSION TECHNOLOGY PROGRAMME

The fusion technology physics work has been performed in close co-operation with other EURATOM Associations, in particular with EURATOM-CCFE, Culham, EURATOM-KIT Karlsruhe and EURATOM-FOM, Petten.

Institute: **ICP UL – Institute of Chemical Physics, University of Latvia**

Research scientists: MSc. Sarmite Kaleja
Dr. Gunta Kizane
Dr. Bronislavs Lescinskis
MSc. Elina Pajuste
BSc. Ingars Reinholds
Dr. Vija Tilika
Dr. Juris Tiliks Jun.
Dr. Aigars Vitins

4.1. Analysis of tritium distribution in carbon-based plasma-facing components

Principal investigator: G.Kizane

INTRODUCTION

Carbon tiles have been widely used for the first wall of the Joint European Torus (JET) and are the candidate material for the lower vertical targets of the divertor plates of ITER.

Carbon based materials are foreseen to be used at the strike point of divertor regions of high thermal conductivity for fusion devices. The ability of carbon to withstand high heat flux and its favorable thermo mechanical properties (carbon sublimates rather than melts during disruptions or edge localized modes), a low atomic number of carbon reduces the detrimental effects of impurities in the plasma.

Control and removal of trapped tritium is very important issue for fusion devices due to the maximum tritium inventory allowed inside of the ITER machine. Retention of tritium in plasma facing materials will limit ITER operation.

Interaction of plasma with the inner wall material of the vacuum vessel causes erosion and formation of deposited/co-deposited layers, mixed materials and spatially non uniform tritium retention. Mechanisms of fuel retention and desorption is not completely clarified. The amount of the accumulated tritium depends of on the materials of a fusion device and of on the plasmas operation conditions. The larger amount of tritium will be co-deposited with carbon based materials. It is important to determine the tritium amount accumulated in the bulk of those tiles and to estimate the conditions that have an effect on that accumulation.

Relatively a large fraction of the total tritium retained by a tile had migrated deep into the bulk of the tile. Analysis of selected samples of plasma-facing components is necessary in order to support particle transport studies. In order to understand the mechanism of tritium retention in carbon fiber composites, it is necessary to the know tritium depth profile.

Goals of the task are to determine depth profiles of tritium trapped in the bulk of CFC tiles, make comparison of tritium activities in the bulk and surface layers, estimate changes of structure of a tile, to investigate properties of the tritium trapped in CFC tiles, to analyze samples by full combustion method, scanning electron microscopy (SEM) and by Raman spectroscopy. The task JW9-FT-3.46 is related to the estimation of the tritium distribution in the carbon based tiles and is continuation of the EFDA JET Technology Tasks JW8-FT-1.12.

EXPERIMENTAL

Tritium distribution and the effect of the structural changes on that have been analyzed in the selected tile of the JET Mark II SRP divertor. The analyzed tile was from JET MkII Septum Replace Plate (SRP) divertor used in 2001-2004 operation periods of JET. In the MkII-SRP divertor the septum structure of the MkII-GB divertor was replacing with a simple carbon fiber plate (Fig. 4.1.1.).

Tile 14BWG4B was selected for realization the task. The tile is made of Carbon Fibre Composite, Concept I manufactured by Dunlop Ltd. The tile is 2D woven fiber and is manufactured from fiber reinforced graphite by chemical vapor deposition with methane.

During the operation period the divertor temperature was held at about 200°C, the backside was cooled and bulk temperature of the tile between pulses was about 100 °C. Tritium in vacuum chamber was introduced by gas puffing, neutral beam injection. In the year 2003 Trace Tritium Experiment had been performed with an introduction of 380 mg tritium into the vacuum chamber. There tritium was as a thermalized T+, fast tritium with energy about 100 KeV and with energy up to 1 MeV as a result of D-D reactions. The integrated ion flux was in order 10^{27} ions.m⁻³, neutron flux was $3.6 \cdot 10^{14}$ n.cm⁻². Estimated that 66 g of deuterium input retained in the vessel, what is approximately 4 % of total deuterium. The tritium accumulation dominates on the inner divertor shadowed areas.

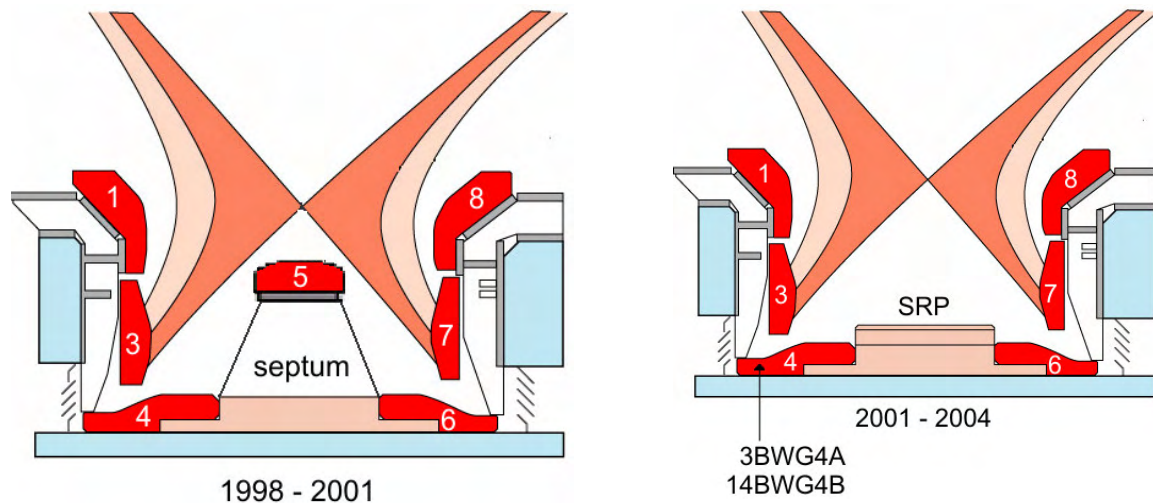


Figure 4.1.1. Configurations of JET divertors Mk-II-GB of the Gas-Box type with a septum (left) and a septum replacement plate (SRP) (right).

Samples for analysis of tritium and structure were made by core-drilling method. Cylinders (\varnothing 1mm) were cut from CFC tiles and sliced into separate disks of thickness 1 mm. In order to determine the tritium content in the separate carbon discs, the full combustion technique was used. Liquid scintillation method was used for measurements of tritium. Analysis of the structure and impurities has been done by the methods of Scanning Electron microscopy, Raman spectroscopy and Energy-dispersive X-ray spectroscopy.

Core drilling positions of tile 14BWG4B for tritium analysis in a poloidal and toroidal direction are shown in Fig. 4.1.2. From tile 14BWG4B cylinders were core-drilled in 11 rows in poloidal and in 6 rows in toroidal directions. Each cylinder was sliced in 11 – 23 slices depending on the width of the tile. Because of technical possibilities and of the differences in exposure conditions, the tile was divided in three parts: septum replace plate (SRP) part (I), sloping part (II) and shadowed part or louvers side part (III). Tritium desorption experiments were realized for samples from plasma exposed side. The technical holes and the places of joint screws of the tile to basement are shown in the Fig. 4.1.3. The slices (A1) of selected cylinders (Cyl1, Cyl4, Cyl5 and Cyl11) were analyzed by the thermodesorption setup up to 1000 C temperatures. The total released tritium activity was calculated by integrating the release rate over the time region where a release is measurable.

The distribution of tritium with depth through the tile has been measured at different toroidal and poloidal positions. A high concentration of tritium was found in the slices at the plasma facing surface. At some tile positions (e.g. at the inner divertor corner shadowed from the plasma) up to 98-99% of the T can be in the surface slice, whereas in other poloidal positions there can be more T in the bulk than at the surface. The tritium distribution in the toroidal and poloidal directions is not uniform; concentration of accumulated tritium strongly depends on the location of the tile.

The changes in position and ratio of the carbon lines (1588 cm^{-1} and 1355 cm^{-1}) in the Raman spectra with depth through each core indicates the degree of disruption of the carbon lattice. The structural changes of the tile material close to the plasma facing surface are considerable and correlation with the tritium accumulation has been observed.

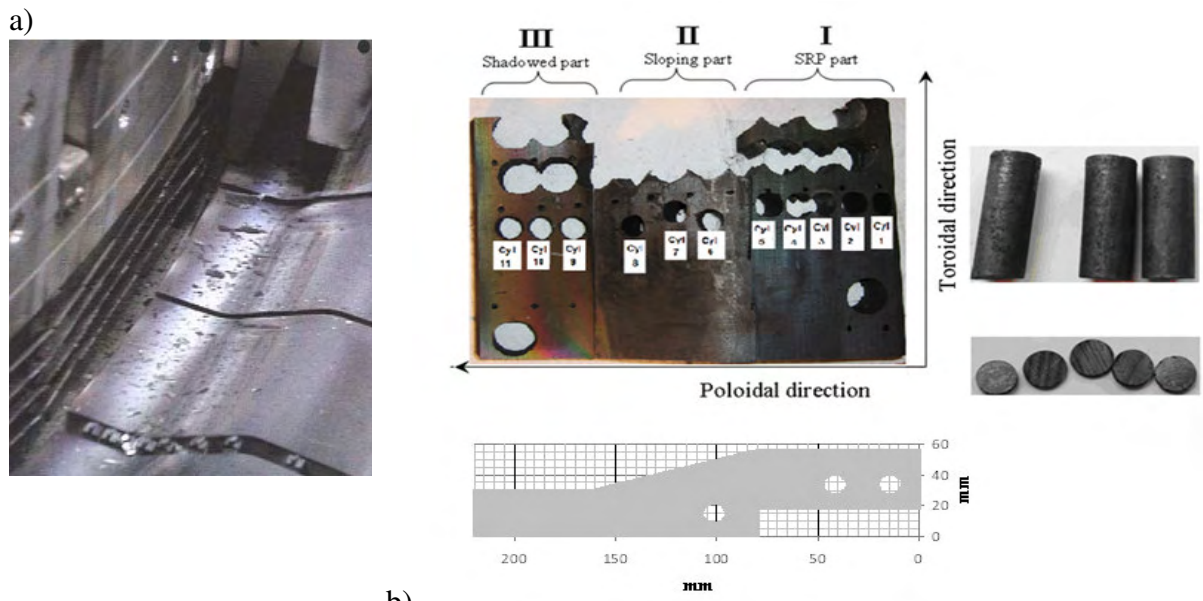


Figure 4.1.2 The tiles (a) of the divertor and (b) core drilling positions of tile 14BWG4B in a poloidal and toroidal direction

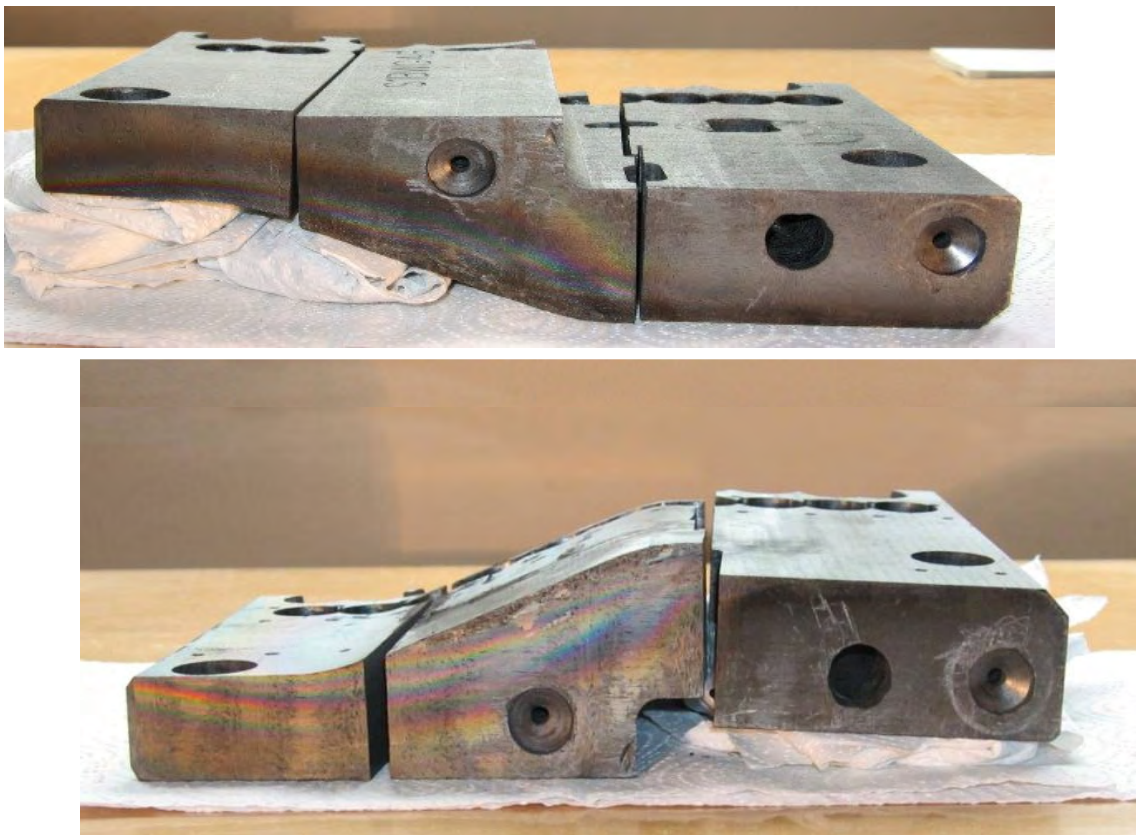


Figure 4.1.3. Side view of tile 14 BWG4B with technical holes from back side and plasma facing side.

Results

DISTRIBUTION OF TOTAL TRITIUM IN CARBON-BASED DISCS

Tritium activity in the surface layers and in the bulk is connected with the thickness of deposition layer and with the energy of plasma deposited on a tile.

The highest surface activities of tritium were found in the shadowed part (III) of the tile. For instance, the mass activity of the surface slice of Cyl10 was $0.156 \text{ GBq}\cdot\text{g}^{-1}$ (Fig.4.1.4), while in Cyl 2 representing the SRP (II) part it was only $0.006 \text{ GBq}\cdot\text{g}^{-1}$.

The shadowed area (III) at a louvers side has a thick deposition layer and no contact with plasma. The shadowed part of the tile 4 is protected by a tile 3.

The sloping part (II) of the tile has the thickest deposition layer up to $300 \mu\text{m}$, but at the same time it has been subjected to high temperature due to the plasma striking the surface and ELM's. Therefore tritium surface activity has similar values to that in the SRP (I) part where the deposition layer is only $10 \mu\text{m}$ or less (Fig.4.1.5.)

Migration of tritium into the bulk of a tile is expected at high temperatures as is clearly demonstrated in the results from the sloping part (II) where the tritium mass activity of the bulk was found to be about an order higher than in other parts of the tile (Fig. 4.1.7.).

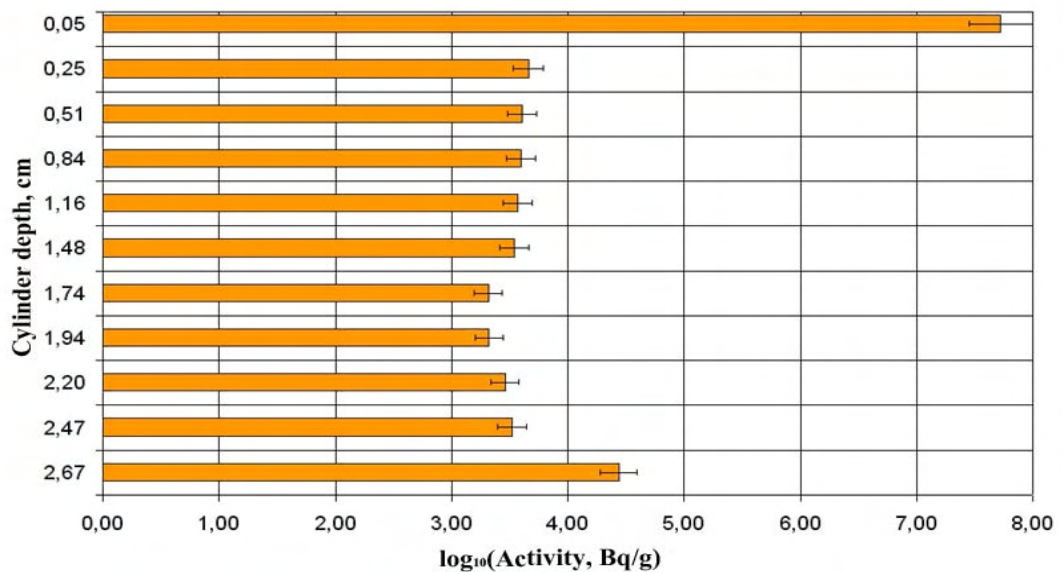


Figure 4.1.4. Depth profiles of mass activity of tritium in cylinder 10 from shadowed part (III) of tile 14BWG4B

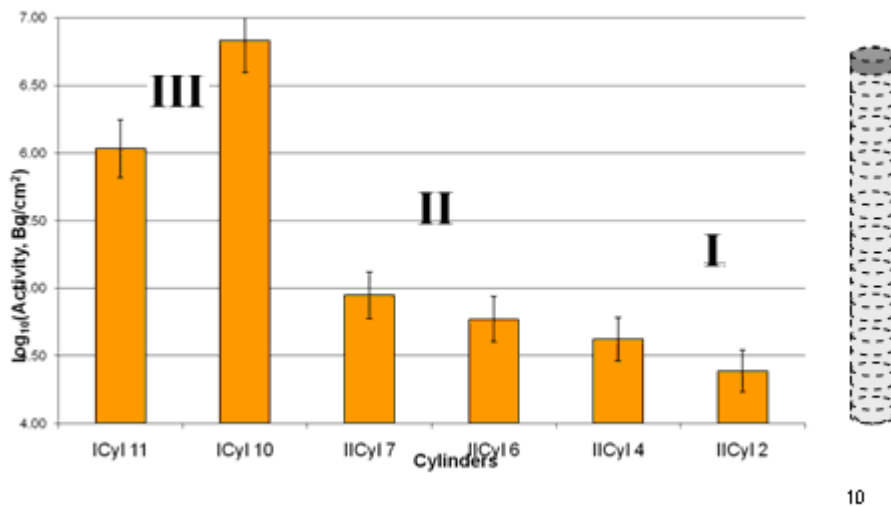


Figure 4.1.5. Surface activity of tritium in different parts of tile 14BWG4B: I – Septum Replace Part (SRP), II – Sloping part and III - Shadowed part at louvers side of tile.

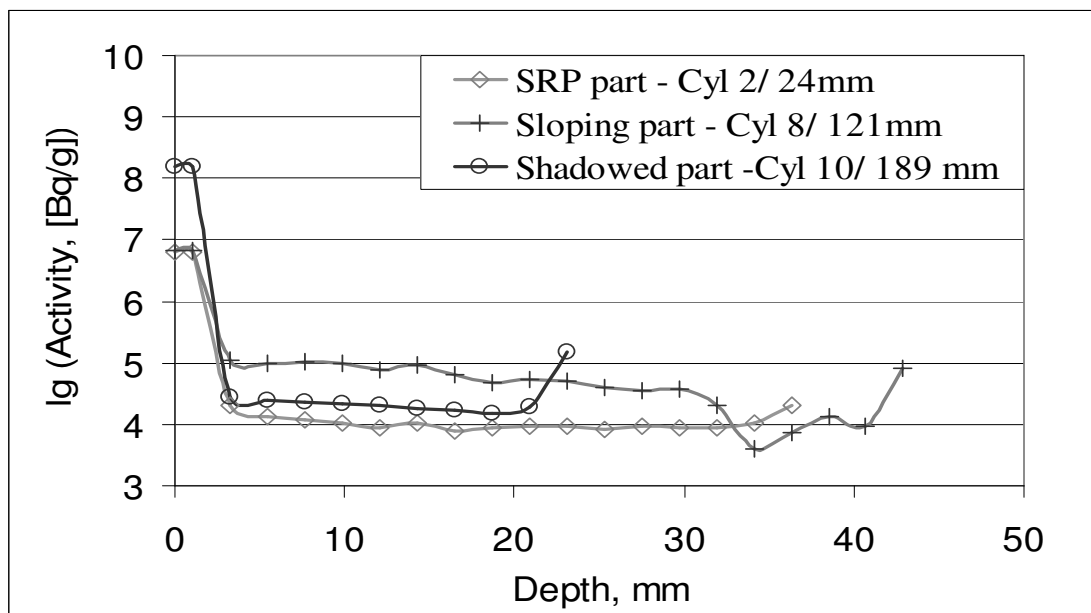


Figure 4.1.6. Depth profiles of tritium in the cylinders from different parts of 14BWG4 tile: Cyl 2 from Septum Replace Plate SRP (I), Cyl 8 from Sloping (II) and Cyl 10 from Shadowed (III) part of the tile.

The carbon fibre modifications were analyzed by SEM in order to understand an increased tritium retention on the backside of a cylinder and in order to clarify are these changes of increased amount of tritium connected with the material structure. An increase of the fibre diameter close to the backside surface was observed to be up to 30% (Figs. 4.1.7., 4.1.8.). There was also a small increase near the plasma facing surface of the SRP part. The co-deposition of tritium and energetic triton implantation

is not possible on the back side of a tile. One of the explanations could be migration of gaseous tritium around the divertor, reaching the backsides of the tiles and adsorption. However the gas pressure in the plasma chamber is extremely low for this mechanism to take place. Observed modifications of fibre have been caused by mechanical forces due to the method of fixing the tile on the divertor.

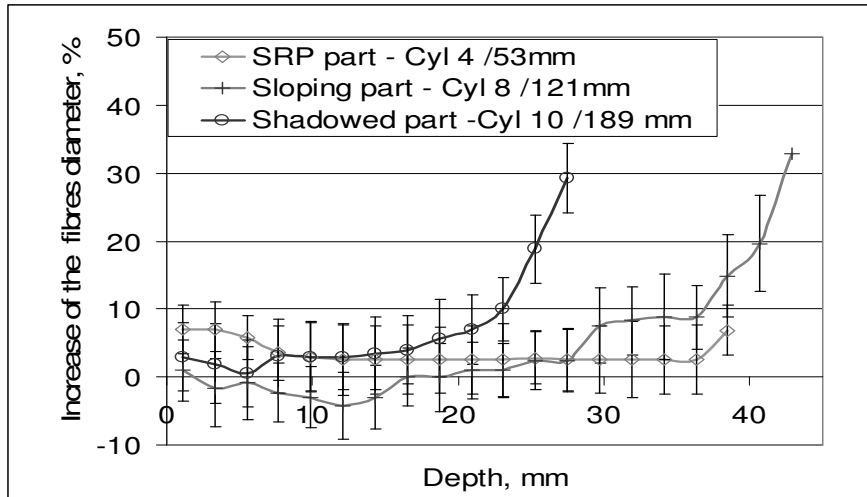


Figure 4.1.7. Changes of the fibre diameter with depth in different parts through of tile 14BWG4B

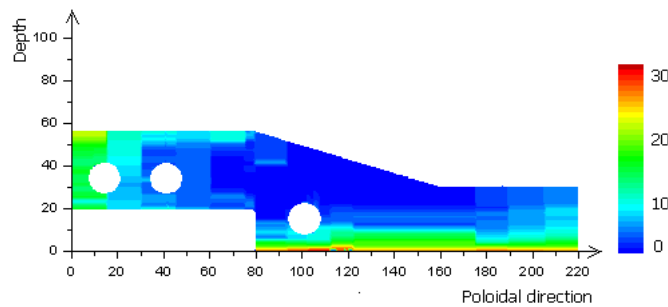


Figure 4.1.8. Schematic cross-section of tile 14BWG4B and a plot showing the increase of the fibre diameter with depth through the tile.

The tile is fixed on a central bolt with the tile supported at the corners, so that the backside is in tension. Therefore, there are no extra graphite planes but existing planes have separated as a result of the deformation, and extra space for tritium to diffuse has appeared. The structure analysis of the tiles confirmed that the largest deformation and contingent destruction of the carbon fibres has occurred in the backside layers. Increase of specific surface area and concentration of trapping sites resulting from destruction of fibres that follows from the 30% radial growth could lead to increased tritium retention.

Carbon fibre composites are inhomogeneous materials, tritium migration and trapping in the fibre matrix, fibre core and sheath are considerable. Therefore, changes of the volume ratio between these components as a result of deformation or/and destruction must have an effect on the tritium penetration and retention process in the bulk. Increase of the space between the sheath graphite planes facilitates the transport of tritium between the planes, while full destruction of fibre sheath leads to the increase of specific surface area and concentration of high energy trapping sites.

It is possible that an increase of the trapping site concentration because of the fracture deformations might be the reason for the higher tritium retention in the backside layer

of the shadowed part of the tile since there the largest structure changes were observed.

Conclusions

1. A common feature for all the cylinders investigated is that most part of tritium is localized in the plasma-facing surface layer, after the amount of tritium sharply decrease, stayed at uniform level and gradually increases from middle part of the cylinder to the end point of the cylinder to the back side of the tile.
2. Layered structure of the fibres and pores between the fibres allows migrating of tritium in the bulk of tile.
3. Increase of the fibre diameter followed by a full destruction of the fibres was observed in the backside layer and could be explained by mechanical forces applied on the tile during exploitation in the divertor. The changes of structure of the fibres might be one of the reasons for increased tritium concentration in the backside layers of a tile.

Results of fusion research were presented at the conferences:

1. The 25th Scientific Conference of Institute of Solid State Physics. University of Latvia, dedicated to commemoration of centenary of Docent Ludvigs Jansons. Riga, February 11-13, 2009.
2. The 25th Scientific Conference of Institute of Solid State Physics. University of Latvia, dedicated to commemoration of centenary of Docent Ludvigs Jansons. Riga, February 11-13, 2009.
3. The 68th Scientific Conference of University of Latvia, Riga, February 11-13, 2009.
4. International Baltic Sea Region Conference “Functional Materials and Nanotechnologies 2009” (FM&NT-2009) Riga, 31st March – 3rd April 2009. – Institute of Solid State Physics, University of Latvia.
5. 12th International Workshop on Plasma-Facing Materials and Components for Fusion Applications. Jülich, Germany, 11th-14th May 2009.
6. 14th International Conference on Fusion Reactor Materials (ICFRM-14), Sapporo, Japan, 05th Sept -15th September 2009.
7. The 9th IAE International Workshop on Beryllium Technology BeWS-9. Almaty, Kazakhstan, 15th Sept -18th September 2009.
8. The 9th International symposium on Fusion Nuclear Technology. Dalian, China, 05th Sept -18th Sept 2009.

5. STAFF MOBILITY ACTIONS

5.1. STAFF MOBILITY VISITS

Gunta Kizane	took part in: <ul style="list-style-type: none">• the EFDA Taskforces and Topical Groups Joint Meeting on Fuelling and Particle Control from 19/03/2009 – 20/03/2009, Garching, Germany;• 1st Progress Meeting on the GOTP “EUROBREED” on 25-28 Mai, 2009.at NRG in Petten, the Netherlands;• EFDA Technical Meeting Assessment of the Status of European Facilities for PSI, 18 June, 2009, Garching, Germany;• 2nd Progress Meeting on the GOTP “EUROBREED” in CEA, Saclay, 16_19Nov, 2009.• in the biannual General Monitoring Meeting to present the status of work under tasks”JW8-FT-1.12” , JW9_FT_3.46” and present an explanation of the background, purpose and objectives of the task JW10_FT_3.62” at the Kick-off Technical meeting. 30Nov/12/2009– 6/12/2009 in the JET Culham Science Centre, Abingdon, UK. Oral presentation
Elina Pajuste	took part in: <ul style="list-style-type: none">• the Karlsruhe Summer school on Fusion Energy in the frame of GOT programme EUROBREED, 29 Aug-09Sept 2009• 2nd Progress Meeting on the GOTP “EUROBREED” in CEA, Saclay, 16_19Nov, 2009.
Olgerts Dumbrajs	FZK Karlsruhe, 27 – 30 April IPP Garching, 1 May - 30 June
Aleksejs Gopejenko	ZFK, Karlsruhe, 26 May – 26 June IPP, Garching, 18 May – 25 May
Jurijs Zukovskis	ZFK, Karlsruhe, 20 September – 3 October
Ivars Tale	IPP, Garching, 18 March – 21 March IPP, Garching, 17 June – 19 June Munich, 05 October – 15 October Warshaw, 3 November – 6 November FTU, Frascati, 26 November – 28 November
Andris Voitkans	IPP, Garching, 04 June – 19 June FTU, Frascati, 26 October -28 October
Mihails Cubarovs	Warshaw, 13 September – 17 September
Olgerts Lielausis	IST,Lisbon, 13 September – 19 September FTU, Frascati, 7 December – 21 December
Aleksejs Klukins	FTU, Frascati, 7 December – 21 December

6. OTHER ACTIVITIES

6.1. CONFERENCES, WORKSHOPS AND MEETINGS

Results of fusion research were presented at the conferences:

1. The 25th Scientific Conference of Institute of Solid State Physics. University of Latvia, dedicated to commemoration of centenary of Docent Ludvigs Jansons. Riga, February 11-13, 2009.
2. The 68th Scientific Conference of University of Latvia, Riga, February 11-13, 2009.
3. International Baltic Sea Region Conference “Functional Materials and Nanotechnologies 2009” (FM&NT-2009) Riga, 31st March – 3rd April 2009. – Institute of Solid State Physics, University of Latvia.
4. 12th International Workshop on Plasma-Facing Materials and Components for Fusion Applications. Jülich, Germany, 11th-14th May 2009.
5. 14th International Conference on Fusion Reactor Materials (ICFRM-14), Sapporo, Japan, 05th Sept -15th September 2009.
6. The 9th IAE International Workshop on Beryllium Technology BeWS-9. Almaty, Kazakhstan, 15th Sept -18th September 2009.
7. The 9th International symposium on Fusion Nuclear Technology. Dalian, China, 05th Sept -18th Sept 2009.

6.2. TELEPHONE CONFERENCES

1. I Semi annual monitoring meeting - JET Fusion Technology on the tasks JW8-1.12-, JW9-FT-3.46 the 5th June 2009.

7. PUBLICATIONS

7.1. FUSION PHYSICS AND PLASMA ENGINEERING

7.1.1. PUBLICATIONS IN SCIENTIFIC JOURNALS

1. R.B.Gomes, H.Fernandes, C.Silva, A.Sarakovskis, T.Pereira, J.Figueiredo, B.Carvalho, A.Soares, P.Duarte, C.Varandas, O.Lielausis, A.Klyukin, E.Platacis, I.Tale, A. Alekseyv ‘Liquid gallium jet-plasma inInteraction studies in ISTTOK tokamak’ , Journal of Nuclear Materials 390-391 (2009) 938-941.
2. R.B.Gomes, H.Fernandes, O.Lielausis, A.Klyukin, E.Platacis, Liquid gallium jet-plasma inInteraction studies in ISTTOK tokamak , Journal of Nuclear Materials 390-391 (2009) 938-941.

7.1.2. CONFERENCE ARTICLES

1. A. Gopejenko, Yu.F. Zhukovskii, P.V. Vladimirov, E.A. Kotomin, and A. Möslang, "Simulation of yttrium and oxygen solute atoms in fcc Fe lattice in support of ODS steel development. 25th ISSP scientific conference (Riga, Latvia, February, 2009). Abstracts: p. 55.
2. A. Gopejenko, Yu.F. Zhukovskii, P. Vladimirov, E.A. Kotomin, and A. Moslang, "Simulations on solution of yttrium and oxygen atoms in fcc iron lattice". International conference "Functional materials and nanotechnologies" FM&NT-2009 (Riga, Latvia, April, 2009), Abstracts: p. 101.
3. A. Gopejenko, Yu.F. Zhukovskii, P.V. Vladimirov, E.A. Kotomin, and A. Möslang, "Simulation of yttrium oxide particle formation in iron in support of ODS steel development". 6th International Conference "Information Technologies and Management", IT&M'2009 (Riga, Latvia, April, 2009). Abstracts: pp. 30-31.
4. D. Constantinescu, O. Dumbrajs, V. Igochine, K. Lackner, R. Meyer-Spasche, H. Zohm "A low-dimensional model system for quasi-periodic plasma perturbations", 13th European Fusion Theory Conference Riga, Latvia, 12-15 October, 2009.
5. O. Dumbrajs, V. Igochine, A. Gude, K. Lackner, M. Maraschek, G. Pereverzev, H. Zohm, and ASDEX Upgrade team, "The role of stochastization in fast MHD phenomena in ASDEX Upgrade, 13th European Fusion Theory Conference Riga, Latvia, 12-15 October, 2009.

7.2. FUSION TECHNOLOGY

7.2.1. PUBLICATIONS IN SCIENTIFIC JOURNALS

1. J.P. Coad, D.E. Hole, E. Kolodinska, J. Likonen, S. Lindig, G.F. Matthews, M. Mayer, V. Philipps, V. Riccardo, A. Widdowson and JET-EFDA contributors Testing of tungsten coatings in JET for the ITER-like wall *Journal of Nuclear Materials*, Volumes 390-391, 15 June 2009, Pages 992-995 DOI:10.1016/j.jnucmat.2009.01.260.
2. J. Tīliks, G. Ķizāne, A. Vītiņš, E. Kolodinska, J. Tīliks Jr., I. Reinholds. Tritium release from beryllium articles for use in fusion devices. – *Journal of Nuclear Materials*. April 2009. Vols. 386–388. Pp. 874–877.
3. J. Tīliks, A. Vītiņš, G. Ķizāne, V. Tīlika, E. Kolodinska, S. Kalēja, B. Leščinskis. Effects of external energetic factors on tritium release from the EXOTIC 8-3/13 neutron-irradiated beryllium pebbles. – *Fusion Engineering and Design*. June 2009. Vol. 84. No. 7-11. Pp. 1842-1846.